

CONCURRENT OBJECT REGRESSION

Satarupa Bhattacharjee and Hans-Georg Müller¹

Department of Statistics, University of California, Davis
Davis, CA 95616 U.S.

(For the Alzheimer's Disease Neuroimaging Initiative²)

December 2020

ABSTRACT

Modern-day problems in statistics often face the challenge of exploring and analyzing complex non-Euclidean object data that do not conform to vector space structures or operations. Examples of such data objects include covariance matrices, graph Laplacians of networks and univariate probability distribution functions. In the current contribution a new concurrent regression model is proposed to characterize the time-varying relation between an object in a general metric space (as response) and a vector in \mathbb{R}^p (as predictor), where concepts from Fréchet regression is employed. Concurrent regression has been a well-developed area of research for Euclidean predictors and responses, with many important applications for longitudinal studies and functional data. We develop generalized versions of both global least squares regression and locally weighted least squares smoothing in the context of concurrent regression for responses which are situated in general metric spaces and propose estimators that can accommodate sparse and/or irregular designs. Consistency results are demonstrated for sample estimates of appropriate population targets along with the corresponding rates of convergence. The proposed models are illustrated with mortality data and resting state functional Magnetic Resonance Imaging data (fMRI) as responses.

KEY WORDS: Metric-space valued data, Fréchet regression, Random Objects, Local regression, Linear model, Varying coefficient model, fMRI, Mortality, ADNI.

¹Research supported by NSF grant DMS-1712864.

²Data used in preparation of this article were obtained from the Alzheimer's Disease Neuroimaging Initiative (ADNI) database (adni.loni.usc.edu). As such, the investigators within the ADNI contributed to the design and implementation of ADNI and/or provided data but did not participate in analysis or writing of this report. A complete listing of ADNI investigators can be found at: http://adni.loni.usc.edu/wp-content/uploads/how_to_apply/ADNI_Acknowledgement_List.pdf

1 INTRODUCTION

Concurrent regression models are an important tool to explore the time-dynamic nature of the dependence between two variables. They are often used in regression problems, where the effect of the covariates on the response variable is affected by a third variable, such as time or age. Specifically, the response at a particular time point is modeled as a function of the value of the covariate only at that specific time point. Concurrent regression models, also known as varying coefficient models, are natural extensions of (generalized) linear models (Hastie and Tibshirani, 1993; Cleveland et al., 2017). Owing to their interpretability and wide applicability in areas such as economics, finance, politics, epidemiology and the life sciences, there exists a rich literature on these models that covers a large range from simple linear models with scalar responses to more complex longitudinal and functional data (Şentürk and Nguyen, 2011; Fan and Zhang, 2008; Ramsay and Silverman, 2005; Şentürk and Müller, 2010; Horváth and Kokoszka, 2012; Wang et al., 2016), including regression problems where both responses and covariate(s) are of functional type.

However, as we enter the era of big data, more complex, often non-Euclidean, data are increasingly observed and this motivates the development of statistical models that are suitable for such complex data. In this paper, we introduce Concurrent Object Regression (CORE) models for very general settings where one is interested in the time-varying regression relation between a response that takes values in a general metric object space without any linear structure and real-valued covariate(s).

For the special case where the observations consist of a paired sample of square integrable random functions $(X(t), Y(t))$ that take values in \mathbb{R} , the linear functional con-

current model is well known (Ramsay and Silverman, 2007) and can be written as

$$E(Y(t)|X(t)) = \mu_Y(t) + \beta(t)(X(t) - \mu_X(t)), \quad (1)$$

where $\mu_Y(\cdot)$ and $\mu_X(\cdot)$ are respectively the mean functions of $X(\cdot)$ and $Y(\cdot)$ and $\beta(\cdot)$ is the smooth coefficient function. This can be thought of as a series of linear regressions for each time point that are connected and restricted by the assumed smoothness of the coefficient function β .

Several methods have been proposed to estimate the model components μ_X, μ_Y and β , which are functional in nature, including local polynomial kernel smoothing regression (Fan and Zhang, 1999, 2000; Hoover et al., 1998; Wu and Chiang, 2000), smoothing splines (Eubank et al., 2004; Chiang et al., 2001) and function approximation of $\beta(\cdot)$ through basis expansion (Huang et al., 2002). These methods were also adapted for spatial imaging (Zhang et al., 2011), ridge regression (Manrique et al., 2018) and other areas. Since the linear approach may not capture the true and possibly complex nature of the relationship between Y and X , the response and the covariate, a more general nonparametric model may be preferable,

$$E(Y(t)|X(t)) = m(t, X(t)), \quad (2)$$

where the regression function m is assumed to satisfy some basic smoothness properties.

Various methods have been discussed for nonparametric functional concurrent regression over the years, including spline smoothing (Maity, 2017), Gaussian process regression (Shi et al., 2007; Wang and Shi, 2014) and local kernel smoothing techniques (Verzelen et al., 2012), with various subsequent developments (Wang et al., 2008; Zhu et al., 2010). Regression methods have also been considered more recently for manifold-valued responses in curved spaces (Zhu et al., 2009; Cornea et al., 2017; Yuan et al., 2013), owing to the

growing realization that data from many disciplines have manifold structures, including data generated in brain imaging, medical and molecular imaging, computational biology and computer vision.

The major objective of this paper is to overcome the limitation of Euclidean responses in the previous concurrent regression approaches, where it is always assumed that $Y \in \mathbb{R}$ or $Y \in \mathbb{R}^p$. The challenge that one faces in extending concurrent regression beyond Euclidean responses is that existing methodology relies in a fundamental way on the vector space structure of the responses, which is no longer available, not even locally, when responses are situated in general separable metric spaces that cover large classes of possible response types. Technological advances have made it possible to record and efficiently store time courses of image, network, sensor or other complex data. Such “object-oriented data” (Marron and Alonso, 2014) or “random objects” (Müller, 2016) can be viewed as random variables taking values in a separable metric space that is devoid of a vector space structure and where only pairwise distances between the observed data are available. As a motivating example for the proposed Concurrent Object Regression (CORE), we consider fMRI brain-image scans for Alzheimer’s patients over varying ages. It is important to note that, the space \mathcal{C} of the functional connectivity network of fMRI signals, represented as correlation matrices between the different nodes of the brain is not linear and there is no concept of direction.

However, the connectivity correlation matrices can be perceived as random objects in a metric space, endowed with a suitable metric. For example, one might be interested to see if certain measures indexing the advancement of the disease, such as the total cognitive score, are associated with the connectivity matrices. It is known that a higher total cognitive score may be linked with a more serious cognitive deficit and a higher age. At the same time, the functional connectivity itself is expected to deteriorate with increasing age as the severity of the condition intensifies over time. Of interest is then

to ascertain the dependence of the functional connectivity correlation matrices of the Alzheimer’s subjects on time (age) and some index of the overall health for the subjects, that also varies over time.

The space of positive semi-definite matrices is a Riemannian Manifold which can be flattened locally and analyzed using linear results, however the Riemannian structure of the space depends on the metric. Our approach of treating it as a metric space is more general in the sense that it works for many metrics in the space such as the Frobenius metric, the log-Euclidean metric (Arsigny et al., 2007), the Procrustes metric (Pigoli et al., 2014; Zhou et al., 2016), the power metric (Dryden et al., 2009, 2010), affine-invariant Riemannian metric (Pennec et al., 2006; Moakher, 2005) the Cholesky metric (Lin, 2019) among others. As such we do not have to evoke the Riemannian geometry of the space, even though a possible challenge inherent in Fréchet regression is to ascertain the existence and uniqueness of the Fréchet mean may be encountered.

Other examples of such general metric space objects include time-varying age-at-death densities resulting from demographic data, where the interest is in quantifying the dynamic regression relationship between the densities and time-dependent some economic index, or time-varying network data, for example internet traffic networks where one has concurrent covariates.

The natural notion of a mean for random elements of a metric space is the Fréchet mean (Fréchet, 1948). It is a direct generalization of the standard mean, and is defined as the element of the metric space for which the expected distance to all other elements is minimized. Petersen and Müller (2019) extended this concept to the notion of a conditional Fréchet mean, implemented as Fréchet regression, where one has samples of data (X_i, Y_i) , with the Y_i being random objects and the X_i are Euclidean predictors. This is an extension of ordinary regression to metric space valued responses.

In Section 2, we introduce the Concurrent Object Regression (CORE) model for time-

varying object responses and time-varying real covariate(s). We separately discuss two situations – one where we assume a “linear” dependence of the predictor and response at any given time point and a second scenario in which we assume a nonparametric model in Sections 3 and 4 respectively. Our motivating application examples deal with samples of probability distributions and correlation matrices, which are illustrated with simulations and real data from neuroimaging, with details in Sections 5 and 6, respectively. We conclude with a brief discussion about our methods in section 7.

2 PRELIMINARIES

Throughout, we consider a totally bounded, separable metric space (Ω, d) , where the response is situated. This is coupled with a p -dimensional real valued stochastic process $X(\cdot)$ as a predictor. The Ω -valued random object response Y depends on both X and a “time”-variable $t \in \mathcal{T}$, where \mathcal{T} is a closed and bounded interval on the real line. In other words, $(X(t), Y(t)) : t \in \mathcal{T}$ are two stochastic processes that, for each given t , take values \mathbb{R}^p and Ω respectively.

A random time T is selected from some distribution f_T on \mathcal{T} , at which X is observed. Note that $X(T)$ is itself a random variable and has a probability distribution on \mathbb{R}^p . The joint distribution of $(X(T), T)$ is well defined in case $X(T)$ and T are independently distributed. For the sake of generality, we consider the joint distribution of $(X(T), T)$ and, with a slight abuse of notation, denote the joint distribution by $F_{(X,T)}$, which is a probability distribution on $\mathbb{R}^p \times \mathbb{R}$. We further assume that $Y \sim F_Y$ where F_Y is a distribution on (Ω, d) . The conditional distributions of $Y(T)|(X(T), T)$ and $(X(T), T)|Y(T)$ are denoted by $F_{Y|(X,T)}$ and $F_{(X,T)|Y}$ respectively, assuming they exist. We define the

Concurrent Object Regression (CORE) model as follows,

$$m_{\oplus}(x, t) := E_{\oplus}(Y(t)|X(t) = x, T = t) := \operatorname{argmin}_{\omega \in \Omega} M_{\oplus}(\omega, x, t),$$

$$M_{\oplus}(\omega, x, t) = E(d^2(Y(t), \omega)|X(t) = x, T = t) \quad (3)$$

and refer to the objective function $M_{\oplus}(\cdot, x, t)$ in (3) as the conditional Fréchet function. Our next goal is to express the CORE function $m_{\oplus}(x, t)$ in (3) as a weighted Fréchet mean, where the weight function varies with the values (x, t) of the predictors. In the following, we consider both a global and a local approach. The intuition behind these approaches derives from the special case of $\Omega = \mathbb{R}$.

For the special case of $\Omega = \mathbb{R}$, equipped with the metric $d(a, b) = d_E(a, b) = |a - b|$ for all $a, b \in \mathbb{R}$, the minimizer of M_{\oplus} in (3) exists, is unique and coincides with the conditional expectation, and we write

$$m_{\oplus}(x, t) = E_{\oplus}(Y(t)|X(t) = x, T = t) = E(Y(t)|X(t) = x, T = t) := m(x, t). \quad (4)$$

For ease of presentation, we provide details for the case of a scalar predictor $X(\cdot) \in \mathbb{R}^p$ when $p = 1$, where extensions to the case $p > 1$ can also be implemented.

In many scenarios one does not fully observe the trajectories of responses $Y(t)$ and covariates $X(t)$. We consider a general situation, where each subject is measured at random time points, possibly according to a sparse design, with observed data of the form $(T_{il}, X_i(T_{il}), Y_i(T_{il})); l = 1, \dots, n_i; i = 1, \dots, n$, i.e., for the i^{th} subject one has observations of the response $Y(\cdot)$ and predictor $X(\cdot)$ at time points T_{il} that may vary from subject to subject. We denote the observed data by $(T_{il}, X_{il}, Y_{il}); l = 1, \dots, n_i; i = 1, \dots, n$.

Local kernel-based nonparametric regression approaches to estimate a smooth regres-

sion function for Euclidean responses have been well investigated due to their versatility and flexibility. If we assume a local relationship of the response Y with the predictors T and X , the local linear estimate of the function m at the point (x_0, t_0) in (4) is given by $\hat{m}(x_0, t_0) := \hat{\beta}_0$. Here,

$$(\hat{\beta}_0, \hat{\beta}_1, \hat{\beta}_2) = \underset{\beta_0, \beta_1, \beta_2}{\operatorname{argmin}} \frac{1}{n} \sum_{i=1}^n \left(\frac{1}{n_i} \sum_{j=1}^{n_i} (Y_{il} - \beta_0 - \beta_1(X_{il} - x_0) - \beta_2(T_{il} - t_0))^2 \right) \times K_{h_1, h_2}(X_{il} - x_0, T_{il} - t_0). \quad (5)$$

K is a bivariate kernel function, which corresponds to a bivariate density function, and h_1, h_2 are the bandwidth parameters such that $K_{h_1, h_2}(x_1, x_2) = (h_1 h_2)^{-1} K(x_1/h_1, x_2/h_2)$. We can view this estimator as an M-estimator of the alternative population target,

$$(\beta_0^*, \beta_1^*, \beta_2^*) = \underset{\beta_0, \beta_1, \beta_2}{\operatorname{argmin}} \int \left[K_{h_1, h_2}(x - x_0, t - t_0) \times \left(\int y dF_{Y|X, T}(y, x, t) - \beta_0 - \beta_1(x - x_0) - \beta_2(t - t_0) \right)^2 \right] dF_{(X, T)}(x, t). \quad (6)$$

Defining

$$\mu_{jk} := E(K_{h_1, h_2}(X - x_0, T - t_0)(X - x_0)^j(T - t_0)^k), \quad (7)$$

$$r_{jk} := E(K_{h_1, h_2}(X - x_0, T - t_0)(X - x_0)^j(T - t_0)^k Y), \quad \Sigma = \begin{bmatrix} \mu_{00} & \mu_{10} & \mu_{01} \\ \mu_{10} & \mu_{20} & \mu_{11} \\ \mu_{01} & \mu_{11} & \mu_{02} \end{bmatrix},$$

the solution of the minimization problem in (6) is

$$\tilde{l}(x_0, t_0) = \beta_0^* = \begin{bmatrix} 1, & 0, & 0 \end{bmatrix} \Sigma^{-1} \begin{bmatrix} r_{00}, & r_{10}, & r_{01} \end{bmatrix} = E(s^L(X, x_0, T, t_0, h_1, h_2)Y), \quad (8)$$

with weight function s^L given by

$$s^L(X, x_0, T, t_0, h_1, h_2) = K_{h_1, h_2}(X - x_0, T - t_0) [\nu_1 + \nu_2(X - x_0) + \nu_3(T - t_0)], \quad (9)$$

$$[\nu_1, \nu_2, \nu_3] = \frac{1}{\sigma_0^2} [\mu_{20}\mu_{02} - \mu_{11}^2, \quad \mu_{01}\mu_{11} - \mu_{02}\mu_{10}, \quad \mu_{10}\mu_{11} - \mu_{20}\mu_{01}],$$

$$\sigma_0^2 = |\Sigma| = (\mu_{00}\mu_{20}\mu_{02} - \mu_{00}\mu_{11}^2 - \mu_{10}^2\mu_{02} - \mu_{01}^2\mu_{20} + 2\mu_{01}\mu_{10}\mu_{11}),$$

where $|A|$ denotes the determinant of any square matrix A . Observing that

$\int s^L(x, x_0, t, t_0, h_1, h_2) dF_{Y, X, T}(y, x, t) = 1$, it follows that $\tilde{l}(x_0, t_0)$ in (8) corresponds to a localized Fréchet mean w.r.t. the Euclidean metric $d_E(a, b) := |a - b|$,

$$\tilde{l}(x_0, t_0) = \operatorname{argmin}_{y \in \mathbb{R}} E(s^L(X, x_0, T, t_0, h_1, h_2) d_E^2(Y, y)). \quad (10)$$

The minimizer $\tilde{l}(x_0, t_0)$ can be viewed as a smoothed version of the true regression function, and can therefore be treated as an intermediate target.

3 NONPARAMETRIC CONCURRENT OBJECT REGRESSION

The local regression concept from the Euclidean case can be readily generalized to the case of an Ω -valued stochastic process $Y(t) : t \in \mathcal{T}$, where Ω denotes a separable metric space. To study (3), we first define an intermediate function $\tilde{l}_\oplus(x_0, t_0)$ at the chosen points (x_0, t_0) , retaining the same weights and replacing the Euclidean metric d_E by d as in (10),

$$\tilde{l}_\oplus(x_0, t_0) := \operatorname{argmin}_{\omega \in \Omega} \tilde{L}_\oplus(\omega), \quad \text{where } \tilde{L}_\oplus(\omega) := E(s^L(X, x_0, T, t_0, h_1, h_2) d^2(Y, \omega)), \quad (11)$$

where s^L is as in (9) and captures the local dependence of the response on the predictor. Minimizing the intermediate objective $\tilde{L}_\oplus(\omega)$ in (11) turns out to be approximately the same as minimizing the final objective $M_\oplus(\omega)$ in (3). Finally, we propose an estimator

for the intermediate target based on the plug-in estimates of the auxiliary parameters by their corresponding empirical estimates.

Defining

$$\hat{\mu}_{jk} := \frac{1}{n} \sum_{i=1}^n \frac{1}{n_i} \sum_{l=1}^{n_i} K_{h_1, h_2}(X_{il} - x_0, T_{il} - t_0)(X_{il} - x_0)^j (T_{il} - t_0)^k, \quad (12)$$

$$\hat{\Sigma} = \begin{bmatrix} \hat{\mu}_{00} & \hat{\mu}_{10} & \hat{\mu}_{01} \\ \hat{\mu}_{10} & \hat{\mu}_{20} & \hat{\mu}_{11} \\ \hat{\mu}_{01} & \hat{\mu}_{11} & \hat{\mu}_{02} \end{bmatrix}, \quad \hat{\sigma}_0^2 = |\hat{\Sigma}|, \quad N = \sum_{i=1}^n n_i, \quad (13)$$

$$[\hat{\nu}_1, \hat{\nu}_2, \hat{\nu}_3] = \frac{1}{\hat{\sigma}_0^2} [\hat{\mu}_{20}\hat{\mu}_{02} - \hat{\mu}_{11}^2, \quad \hat{\mu}_{01}\hat{\mu}_{11} - \hat{\mu}_{02}\hat{\mu}_{10}, \quad \hat{\mu}_{10}\hat{\mu}_{11} - \hat{\mu}_{20}\hat{\mu}_{01}], \quad (14)$$

$$\hat{s}_{il}(x_0, t_0, h_1, h_2) = K_{h_1, h_2}(X_{il} - x_0, T_{il} - t_0) [\hat{\nu}_1 + \hat{\nu}_2(X_{il} - x_0) + \hat{\nu}_3(T_{il} - t_0)], \quad (15)$$

plugging in the above empirical estimates we obtain the local Fréchet regression estimate

$$\hat{l}_\oplus(x_0, t_0) := \underset{\omega \in \Omega}{\operatorname{argmin}} \hat{L}_\oplus(\omega), \quad \hat{L}_\oplus(\omega) := \frac{1}{n} \sum_{i=1}^n \frac{1}{n_i} \sum_{l=1}^{n_i} \hat{s}_{il}(x_0, t_0, h_1, h_2) d^2(Y_{il}, \omega). \quad (16)$$

Under suitable assumptions the bias introduced by changing the true target in (3) to the intermediate target in (11), given by $d(m_\oplus(\cdot, \cdot), \tilde{l}_\oplus(\cdot, \cdot))$, converges to 0 as the bandwidths $h_1, h_2 \rightarrow 0$. In addition the stochastic term $d(\hat{l}_\oplus(\cdot, \cdot), \tilde{l}_\oplus(\cdot, \cdot))$, converges to 0 in probability, which then yields the convergence of the proposed plug-in estimator in (16) to the true target model in (3). To establish this, we require the following assumptions, which are similar to assumptions in Petersen and Müller (2019).

(A1) The kernel K is symmetric around zero, with $|K_{jk}^\gamma| = |\int K(u, v) u^k v^\gamma du dv| < \infty$ for all $j, k = 1, \dots, 6$ and $\gamma = 0, 1, 2$. Also there is a common bandwidth parameter $h > 0$, $h \rightarrow 0$, $nh \rightarrow \infty$ as $n \rightarrow \infty$, such that $h_1, h_2 = O(h)$ and

$$h = O(\max(h_1, h_2)).$$

(A2) The marginal density $f_{(X,T)}(x, t)$ and the conditional density $f_{(X,T)|Y}(x, t, y)$ exist and are twice continuously differentiable as a bivariate function of (x, t) , the latter for all y .

(A3) The Fréchet means $m_{\oplus}(x_0, t_0)$, $\tilde{l}_{\oplus}(x_0, t_0)$, $\hat{l}_{\oplus}(x_0, t_0)$ exist and are unique.

(A4) For any $\epsilon > 0$, $\liminf_n \inf_{d(\omega, m_{\oplus}(x_0, t_0)) > \epsilon} (M_{\oplus}(\omega, x_0, t_0) - M_{\oplus}(m_{\oplus}(x_0, t_0), x_0, t_0)) > 0$ and $\inf_{d(\omega, \tilde{l}_{\oplus}(x_0, t_0)) > \epsilon} (\tilde{L}_{\oplus}(\omega, x_0, t_0) - \tilde{L}_{\oplus}(\tilde{l}_{\oplus}(x_0, t_0), x_0, t_0)) > 0$.

(A5) The metric space Ω is totally bounded and separable and there exist constants $\eta_1 > 0$, $C_1 > 0$, with $d(\omega, m_{\oplus}(x_0, t_0)) < \eta_1$ such that

$$M_{\oplus}(\omega, x_0, t_0) - M_{\oplus}(m_{\oplus}(x_0, t_0), x_0, t_0) \geq C_1 d(\omega, m_{\oplus}(x_0, t_0))^2.$$

(A6) There exist $\eta_2 > 0$, $C_2 > 0$, with $d(\omega, \tilde{l}_{\oplus}(x_0, t_0)) < \eta_2$ such that

$$\liminf_n [\tilde{L}_{\oplus}(\omega, x_0, t_0) - \tilde{L}_{\oplus}(\tilde{l}_{\oplus}(x_0, t_0), x_0, t_0)] \geq C_2 d(\omega, \tilde{l}_{\oplus}(x_0, t_0))^2.$$

(A7) Denoting the ball of radius δ centered at $m_{\oplus}(x, t)$ by $\mathcal{B}_{\delta}(m_{\oplus}(x, t)) \subset \Omega$ and its covering number using balls of size ϵ as $N(\epsilon, \mathcal{B}_{\delta}(m_{\oplus}(x, t)), d)$, $\int_0^1 \sqrt{1 + \log N(\epsilon, \mathcal{B}_{\delta}(m_{\oplus}(x, t)), d)} d\epsilon = O(1)$ as $\delta \rightarrow 0$.

Assumptions (A1)-(A2) are necessary to show that the intermediate objective function \tilde{L}_{\oplus} is a smoothed version of the true objective function M_{\oplus} . These are assumptions akin to the ones made in [Petersen and Müller \(2019\)](#) and are common in the nonparametric regression literature. Assumption (A3) is regarding the existence and uniqueness of the Fréchet means. The existence of the Fréchet means depends also on the nature of the space, as well as the metric considered. For example, in a Euclidean space the Fréchet means coincide with the usual means for random vectors with finite second moments. In case of Riemannian manifolds the existence, uniqueness, and the convexity of the center

of mass is guaranteed (Afsari, 2011; Pennec et al., 2018). In a space with a negative or 0 curvature, or in a Hadamard space the existence and uniqueness of the Fréchet means are also shown (Bhattacharya et al., 2003; Bhattacharya and Patrangenaru, 2005; Patrangenaru and Ellingson, 2015; Sturm, 2003; Kloeckner, 2010).

For each such space and a suitable metric, the computation to find the Fréchet means could be different, giving the methods more flexibility. In many cases, the key idea to find the weighted Fréchet means reduces to solving a constrained quasi-quadratic optimization problems and projecting back into the solution space. For a wide class of objects such as distributions, positive semi-definite matrices, networks, and Riemannian manifolds among others, the existence of the unique solution can be found analytically (see Propositions 1 and 2 in the Appendix of Petersen and Müller (2019)), and is not computationally difficult to obtain.

Assumptions (A3)-(A4) are commonly invoked to establish consistency of an M-estimator such as $\hat{m}_\oplus(x_0, t_0)$, where one uses the weak convergence of the empirical process \hat{L}_\oplus to \tilde{L}_\oplus , which in turn converges smoothly to M_\oplus . Assumptions (A5)-(A6) relate to the curvature of the objective function and are needed to control the behavior of $\tilde{L}_\oplus - M_\oplus$ and $\hat{L}_\oplus - \tilde{L}_\oplus$ respectively, near the minimum. Assumption (A7) gives a bound on the covering number of the object metric space and is satisfied by the common examples of random objects such as distributions, covariance matrices, networks and so on.

In the concurrent regression framework, an important feature of the predictor space is as follows: when $X(t) \in \mathbb{R}^p$, for any given $t \in \mathcal{T}$, the set $\{(t, X(t)) : t \in \mathcal{T}\}$ is a p -dimensional manifold \mathcal{M} embedded in the ambient space \mathbb{R}^{p+1} . This reduces the effective dimension of the predictor space from $p+1$ to p . The observed data (T_{il}, X_{il}) take values on this p -dimensional manifold embedded in \mathbb{R}^{p+1} . Note that this does not contradict our assumptions regarding the existence of the joint densities, $f_{X,T}$ (Section 2).

Denoting by $\mathcal{B}_r^k(a) \subset \mathbb{R}^k$ a ball in \mathbb{R}^k with center $a \in \mathbb{R}^k$ and radius $r > 0$, for any

$t_0 \in \mathcal{T}$, the center of the ball $\mathcal{B}_h^{p+1}(t_0, X(t_0))$ is situated on the manifold \mathcal{M} . The following assumptions ensure that the predictors are dense on \mathcal{M} .

(A8) Assume that for any $t_0 \in \mathcal{T}$, the number of sample points outside balls $\mathcal{B}_h^{p+1}(t_0, X(t_0))$ is bounded by

$$E \left(K^\gamma \left(\frac{X-x_0}{h}, \frac{T-t_0}{h} \right) \mathbf{1} \left((T, X(T)) \notin \mathcal{B}_h^{p+1}(t_0, X(t_0)) \right) (X - x_0)^j (T - t_0)^k \right) = o(h^{p+j+k}),$$

for $\gamma = 0, 1, 2$, where $\mathbf{1}(z \notin A)$ denotes the indicator function for an element z not belonging to a set A .

(A9) The density $f_T(\cdot)$ of T is bounded away from 0 and for some constant $c_{t_0} > 0$, $\lim_{n \rightarrow \infty} E(\#\text{sample points falling inside } \mathcal{B}_h(t_0, X(t_0)))/(nh) = c_{t_0}$.

Assumptions (A8)-(A9) concern the existence of a local “chart” or homeomorphism from the neighborhood in the predictor space \mathbb{R}^{p+1} to a ball in \mathbb{R}^p , along the curve \cdot . The manifold structure of the predictor space is crucial to show that the rate of convergence corresponds to that for p -dimensional predictors even though the predictor dimension is \mathbb{R}^{p+1} .

For the remainder of this section we will assume that $X(t) \in \mathbb{R}^p$, where $p = 1$ for all $t \in \mathcal{T}$, that is the dimension of the predictor space $(T, X(T))$, for any random time point T is $p+1 = 2$. This allows for simpler notation and implementation. At the cost of much more involved notation, the theory can be extended to cover cases where $p > 1$.

Proposition 1. *Under the regularity assumptions (A1)-(A6)*

$$d(m_{\oplus}(x, t), \tilde{l}_{\oplus}(x, t)) = O(h^2), \quad \text{as } h = h_n \rightarrow 0 \text{ and } nh \rightarrow \infty \text{ where } h \text{ is as in (A1).}$$

Proposition 2. *Under the regularity assumptions (A1)-(A9)*

$$d(\hat{l}_\oplus(x_0, t_0), \tilde{l}_\oplus(x_0, t_0)) = O_p((nh)^{-1/2}), \text{ as } h = h_n \rightarrow 0 \text{ and } nh \rightarrow \infty \text{ where } h \text{ is as in (A1).}$$

Proposition 1 and 2 demonstrate that, while we have a *two dimensional* predictor (X, T) , the rate of convergence of the proposed estimator still corresponds to the known optimal rate for a nonparametric regression with a *one-dimensional* predictor. A similarly reduced rate of convergence is obtained for a p -dimensional Euclidean predictor X . The reason that the effective predictor dimension is p and not $(p+1)$ is the manifold constraint. In general, the rate of convergence is dictated by the local geometry of the object space near the minimum as quantified in (A4)-(A6). The derivations for the pointwise results are in Appendix A1 and like Theorem 3 and Theorem 4 of Petersen and Müller (2019) rely on tools from the theory of M-estimation. Combining these two results leads to

Theorem 1. *Under the regularity conditions (A1)-(A9),*

$$d(m_\oplus(x_0, t_0), \hat{l}_\oplus(x, t)) = O_p\left(h^2 + (nh)^{-\frac{1}{2}}\right) \text{ as } h = h_n \rightarrow 0 \text{ and } nh \rightarrow \infty.$$

Under the Assumptions (A1)-(A9), if we consider a sequence of bandwidths of the form $h = n^{-\gamma}$, the optimal choice for γ that minimizes the mean square error is obtained for $\gamma^* = 1/5$ and the resulting rate of convergence is $d(m_\oplus(x_0, t_0), \hat{l}_\oplus(x, t)) = O_p(n^{-2/5})$.

The nonparametric models considered so far are subject to the curse of dimensionality for larger dimensions and also require a tuning parameter. Under more stringent modeling assumptions some of these issues can be avoided by a modeling approach that extends the notion of linear relationship to the X direction and will be discussed next.

4 PARTIALLY GLOBAL CONCURRENT OBJECT REGRESSION

In the Euclidean case, a well-established alternative to nonparametric concurrent regression is a varying coefficient model, where for each fixed time a linear regression of $Y(\cdot)$ on $X(\cdot)$ is assumed. This linear regression relation can be described by a global weight function applied to the covariate $X(\cdot)$. This can then be adapted for the case where responses are random objects by constructing conditional Fréchet means with this same weight function (Petersen and Müller, 2019), all while assuming nonlinear dependence between $Y(\cdot)$ and T . As before, we first study the special case of a Euclidean response and then express the CORE function in (3) as an intermediate target expressed as a weighted Fréchet mean, the weights being globally linear in the X -direction and locally linear in the T -direction. This leads to the proposed Partially Global CORE model,

$$\tilde{g}_\oplus(x, t_0) = \underset{\omega \in \Omega}{\operatorname{argmin}} \tilde{G}_\oplus(\omega), \quad \text{where } \tilde{G}_\oplus(\omega) := E(s^G(X, x, T, t_0, h) d^2(Y, \omega)). \quad (17)$$

Here the weight function s^G is given by

$$s^G(z, x, t, t_0, h) = s_1(z, x, t, t_0, h) + s_2(t, t_0, h), \quad (18)$$

with $s_1(z, x, t, t_0, h) := K_h(t - t_0) [(z - \mu)^\top \Sigma_{20}^{-1} (x - \mu)]$ and $s_2(t, t_0, h) := \frac{1}{\sigma_0^2} K_h(t - t_0) (\mu_{02} - (t - t_0)\mu_{01})$ with $\mu = E_{X|T}(X)$.

The weight function s^G encapsulates the dependence of the response on the predictors, where the dependence is global in the direction of the covariate X , while it is local in the T direction, which is reflected in the two parts $s^G(X, x, T, t_0, h) = s_1(X, x, T, t_0, h) + s_2(T, t_0, h)$. Observe that $s_1(\cdot, \mu, \cdot, \cdot, \cdot) = 0$, that is, the regression model reduces to a

nonparametric regression model with the only predictor T when $x = \mu$. We see that,

$$\int s_1(z, x, t, t_0, h) dF_{(X,T)}(x, t) = 0.$$

Also, under mild assumptions (Assumption B1 in Appendix A3) on the kernel $K_h(\cdot)$ and the smoothness of marginal and conditional densities $f_{(X,T)}$ and $f_{(X,T)|Y}$ we can show that (see Appendix A4),

$$\int s_2(t, t_0, h) dF_{X,T|Y}(x, t, y) = \frac{dF_{X,T|Y}(x, t, y)}{dF_{X,T}(x, t)} + O(h^2).$$

Thus we may view \tilde{G}_\oplus as a smoothed version of M_\oplus as the bandwidth parameter $h = h_n \rightarrow 0$ (see Appendix A4).

Finally, we propose a plug-in estimate for the regression model m_\oplus in (23). For this purpose we define the preliminary estimates of the auxiliary parameters as follows,

$$\hat{\mu}_{0j} := \frac{1}{n} \sum_{i=1}^n \left(\frac{1}{n_i} \sum_{l=1}^{n_i} K_h(T_{il} - t_0)(T_{il} - t_0)^j \right), \quad (19)$$

$$\hat{\Sigma}_{2j} := \frac{1}{n} \sum_{i=1}^n \left(\frac{1}{n_i} \sum_{l=1}^{n_i} K_h(T_{il} - t_0)(T_{il} - t_0)^j (X_{il} - \bar{X}_l)(X_{il} - \bar{X}_l)^T \right), \quad (20)$$

$$\hat{\sigma}_0^2 := \hat{\mu}_{02}\hat{\mu}_{00} - \hat{\mu}_{01}^2, \quad \hat{\mu} = \bar{X}_l := \frac{1}{n} \sum_{i=1}^n X_{il} \quad (21)$$

and then calculate empirical weights using the auxiliary parameters from above, as,

$$\hat{s}_{il}(x, t_0, h) = K_h(T_{il} - t_0) \left[(X_{il} - \bar{X}_l)^T \hat{\Sigma}_{20}^{-1} (x - \bar{X}_l) + \frac{1}{\hat{\sigma}_0^2} (\hat{\mu}_{02} - (T_{il} - t_0)\hat{\mu}_{01}) \right]. \quad (22)$$

The proposed Partially Global Concurrent Object Regression (CORE) estimate is then

$$\hat{g}_\oplus(x, t) = \operatorname{argmin}_{\omega \in \Omega} \hat{G}_\oplus(\omega), \quad \text{where } \hat{G}_\oplus(\omega) = \frac{1}{n} \sum_{i=1}^n \left(\frac{1}{n_i} \sum_{l=1}^{n_i} \hat{s}_{il}(x, t_0, h) d^2(Y_{il}, \omega) \right). \quad (23)$$

Further motivation of this approach, starting from the case of Euclidean responses, can be found in Appendix A2.

We show consistency with an optimal rate for the proposed model to the target CORE function in (3) under assumptions (B1)-(B6) (see Appendix A3), which are similar to the assumptions (A1)-(A6) in Section 3.

Proposition 3. *Under the assumptions (B1)-(B3) ,*

$$d(m_{\oplus}(x, t_0), \tilde{g}_{\oplus}(x, t_0)) = O(h^2) \text{ as } h = h_n \rightarrow 0.$$

Proposition 4. *Under the assumptions (B1)-(B6),*

$$d(\hat{g}_{\oplus}(x, t_0), \tilde{g}(x, t_0)) = O_p((nh)^{-1/2}) \text{ as } h = h_n \rightarrow 0 \text{ and } nh \rightarrow \infty.$$

Combining these two results leads to the pointwise consistency for the Partially Global CORE estimator,

Theorem 2. *Under (B1)-(B6),*

$$d(\hat{g}_{\oplus}(x, t_0), m_{\oplus}(x, t_0)) = O_p(h^2 + (nh)^{-1/2}) \text{ as } h = h_n \rightarrow 0 \text{ and } nh \rightarrow \infty.$$

Comparing to the local rates of convergence for the Nonparametric CORE estimator, as proposed in Section 3, the rates in Propositions 3 and 4 are global in the predictor X and remain unchanged even for a higher predictor dimension p , $p > 1$. For $p = 1$, both the estimators behave in a similar manner, however as p increases the Partially Global estimator performs better in terms of the rate of convergence to the true CORE model in (3). While the above results are pointwise, a uniform convergence result in a compact interval in the X -direction also holds for any given point in the T -direction, under slightly stronger assumptions (see assumptions (U1)-(U4) in Appendix A3). Denoting the Euclidean norm on \mathbb{R}^p by $\|\cdot\|_E$, we obtain

Theorem 3. *Under the assumptions (U1)-(U4), for any given $t_0 \in \mathbb{R}$ and $M > 0$, as $h = h_n \rightarrow 0$ and $nh \rightarrow \infty$,*

$$\sup_{\|x\|_E \leq M} d(\hat{g}_\oplus(x, t_0), m_\oplus(x, t_0)) = O_p((nh)^{-1/2+\delta}) \text{ for any } \delta > 0.$$

The proof requires results from empirical process theory (see appendix A4).

5 SIMULATION STUDIES

We illustrate the efficacy of the proposed methods through simulations, where the space of distributions with the Wasserstein metric, d_W , provides an ideal setting. We consider time-varying distributions on a bounded domain \mathcal{T} as the response, $Y(\cdot)$, and they are represented by the respective quantile functions $Q(Y)(\cdot)$. The time-varying Euclidean random variable $X(\cdot)$ is taken as the predictor. The random response is generated conditional on $(X(T), T)$, by adding noise to the true regression quantile

$$Q(m_\oplus(x, t))(\cdot) = E(Q(Y)(\cdot)|X(t) = x, T = t). \quad (24)$$

Two different simulation scenarios are examined as we generate the distribution objects from location-scale shift families (see Table 5). In the first setting, the response is generated, on average, as a normal distribution with parameters that depend on $X(T)$ and T . For $(T = t, X(T) = x)$, the distribution parameters $\mu \sim N(\zeta(x, t), \nu_1)$ and $\sigma \sim \text{Gamma}\left(\frac{\eta^2(x, t)}{\nu_2}, \frac{\nu_2}{\eta^2(x, t)}\right)$ are independently sampled, and the corresponding distribution is given by $Q(Y)(\cdot) = \mu + \sigma\Phi^{-1}(\cdot)$. Here, the relevant sub-parameters are $\nu_1 = 0.1$, $\nu_2 = 0.25$, $\zeta(x, t) = 0.1 + 0.2x + 0.5t^2$, and $\eta(x, t) = 0.6 + 0.2x + 0.2\sin(10\pi t)$, and $\Phi(\cdot)$ is the standard normal distribution function. The second setting is slightly more complicated. The distributional parameter $\mu|(X(t) = x, T = t)$ is sampled as before and $\sigma = 0.1$ is assumed to be a fixed parameter. The resulting distribution is then “transported” in

Setting I	Setting II
$Q(Y)(\cdot) = \mu + \sigma\Phi^{-1}(\cdot)$, where $\mu \sim N(\zeta(x, t), \nu_1)$ $\sigma \sim \text{Gamma}\left(\frac{\nu^2(x, t)}{\nu_2}, \frac{\nu_2}{(\nu^2(x, t))}\right)$	$Q(Y)(\cdot) = T\#(\mu + \sigma\Phi^{-1}(\cdot))$, where $\mu \sim N(\zeta(x, t), \nu_1)$ $\sigma = 0.1$, $T_k(a) = a - \sin(ka)/ a , k \in \{\pm 1, \pm 2\}$

Wasserstein space via a random transport maps T , that is uniformly sampled from the collection of maps $T_k(a) = a - \sin(ka)/|k|$ for $k \in \{\pm 1, \pm 2\}$. The distributions thus generated are not Gaussian anymore due to the transportation. Nevertheless, one can show that the Fréchet mean is exactly $\mu + \sigma\Phi^{-1}(\cdot)$ as before.

To this end, we generate a random sample of size n of time-varying response and predictors from the true models, where the i^{th} sample is observed at n_i random time points, incorporating measurement error as described in the two situations above. We sample the time points $T_l \stackrel{i.i.d.}{\sim} \text{Unif}(0, 1)$ and conditionally the predictors $X_i(T_l) \stackrel{i.i.d.}{\sim} \text{Beta}(2, 2)$; $l = 1, \dots, n_i$; $i = 1, \dots, n$. For each setting, 500 Monte Carlo runs were executed for a combination of sample sizes n and n_i , including both sparse and dense designs. For the r^{th} simulation, $\hat{f}_\oplus^r(x, t)$ denoting the fitted distribution function, the utility of the estimation was measured quantitatively by the integrated squared errors,

$$\text{ISE}_r = \int_{-1}^1 \int_0^1 d_W^2(\hat{f}_\oplus^r(x, t), f_\oplus(x, t)) dt dx. \quad (25)$$

We fitted both of the Nonparametric and Partially Global Concurrent Object Regression (CORE) models and compared their performances to a baseline linear concurrent model, which is mis-specified in our case (See Figure A1). As such, in the first setting, where we know the finite-dimensional generating model, we compute the mean $\mu_i(T_l)$ and standard deviation $\sigma_i(T_l)$ of the distribution $Y_i(T_l)$ and regress them linearly against $(X_i(T_l), T_l)$. Both the CORE models perform better than the baseline linear model. Further, the Partially Global CORE has slightly lower ISE value than the Nonparametric one. This is

expected since in this simulation setting, the global model holds true.

In the second simulation setting, the linear model is no longer admissible due to the random transportation step, however, we can still compare the performances between the two proposed CORE models. Both CORE methods performed in a similar manner. We observe a decreasing pattern of the integrated squared errors for increasing sample sizes and denser designs, demonstrating the validity of the CORE models for this complex and time-varying regression setting. The bandwidths for the estimation in both the settings were chosen using a cross validation criterion so as to minimize the average ISE for all simulations.

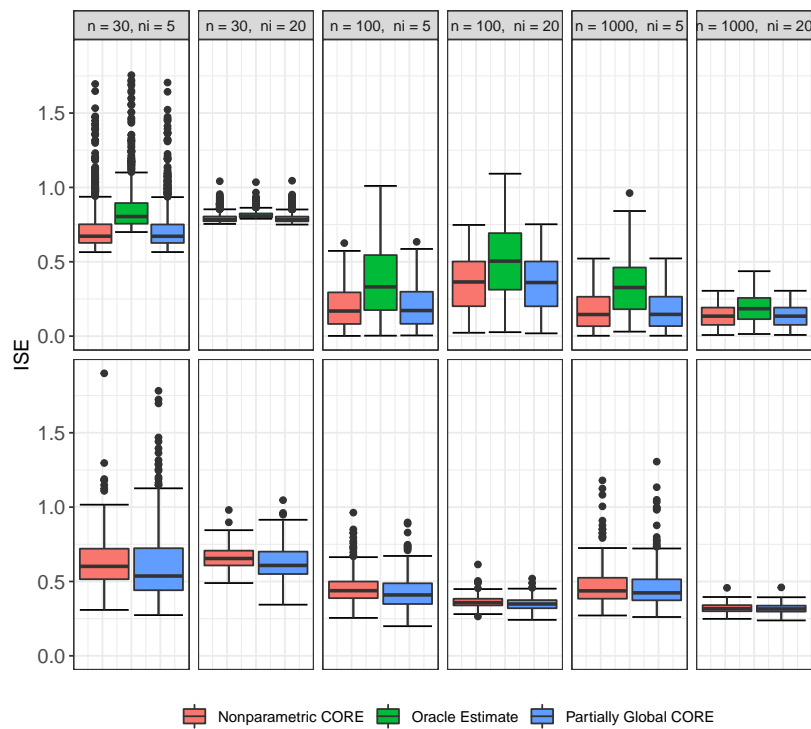


Figure A1: Boxplots of Integrated Squared Errors (ISE) for 500 simulation runs and different sample sizes for density estimates resulting from Partially Global and Nonparametric Concurrent Object Regression (CORE). The upper and lower row show the boxplots for Setting I and Setting II respectively, as described in Table 5.

6 DATA ILLUSTRATIONS

6.1. Brain Connectivity in Alzheimer's Disease

Modern functional Magnetic Resonance Imaging (fMRI) methodology has made it possible to study structural elements of the brain and identify brain regions or cortical hubs that exhibit similar behavior, especially when subjects are in the resting state (Allen et al., 2014; Ferreira and Busatto, 2013).

In resting state fMRI, a time series of Blood Oxygen Level Dependent (BOLD) signal is observed for the seed voxels in selected functional hubs. For each hub, a seed voxel is identified as the voxel whose signal has the highest correlation with the signals of nearby voxels.

Alzheimer's Disease has been found to have associations with anomalies in functional integration of brain regions and target regions or hubs of high connectivity in the brain (Damoiseaux et al., 2012; Zhang et al., 2010).

Data used in the preparation of this article were obtained from the Alzheimer's Disease Neuroimaging Initiative (ADNI) database (adni.loni.usc.edu). For up-to-date information, see www.adni-info.org. Brain image-scans for subjects in different stages of the disease were available, along with other relevant information such as age, gender, and total cognitive score, recorded on the same date as the scan.

For this analysis, only elderly subjects aged from 55 to 90 years and belonging to either of the Alzheimer's Disease (AD) or Cognitive Normal (CN) patient groups were considered. After removing the outliers, the number of image scans recorded were 174 and 694, respectively, for the 78 AD subjects and 371 CN subjects who participated in the study. To confirm that the age intervals across the two groups are comparable, we first performed a Kruskal-Wallis test for the null hypothesis of equal age distributions of the two groups, which resulted in a p-value of 0.92, indicating no evidence for systematic

age differences.

BOLD signals for $V = 10$ brain seed voxels for each subject were extracted. The 10 hubs where the voxels are situated are labeled as follows: LMF and RMF (left and right middlefrontal), LPL and RPL (left and right parietal), LMT and RMT (left and right middle temporal), MSF (medial superior frontal), MP (medial prefrontal), PCP (posterior cingulate/precuneus) and RS (right supramarginal), as discussed in [Buckner et al. \(2009\)](#).

The preprocessing of the BOLD signals was implemented by adopting the standard procedures of slice-timing correction, head motion correction and normalization and other standard steps. The signals for each subject were recorded over the interval $[0, 270]$ (in seconds), with $K = 136$ measurements available at 2 second intervals. From this the temporal correlations were computed to construct the connectivity correlation matrix, also referred to as the Pearson correlation matrix in the area of fMRI studies.

The observations were available sparsely at random time-points, such that the i^{th} subject is observed at n_i time-points, n_i varying from a minimum of 1 to a maximum of 7. The inter-hub connectivity Pearson correlation matrix Y_{il} , for the i^{th} subject observed at age T_{il} (measured in years), has the $(q, r)^{\text{th}}$ element

$$(Y_{il})_{qr} = \frac{\sum_{p=1}^K (s_{ipq} - \bar{s}_{iq})(s_{ipr} - \bar{s}_{ir})}{\left[\left(\sum_{p=1}^K (s_{ipq} - \bar{s}_{iq})^2 \right) \left(\sum_{p=1}^K (s_{ipq} - \bar{s}_{iq})^2 \right) \right]^{1/2}}, \quad (26)$$

where s_{ipq} is the $(p, q)^{\text{th}}$ element of the signal matrix for the i^{th} subject and $\bar{s}_{iq} := \frac{1}{K} \sum_{p=1}^K s_{ipq}$ is the mean signal strength for the q^{th} voxel.

For Alzheimer's disease trials, ADAS-Cog-13 is a widely-used measure of cognitive performance. It measures impairments across several cognitive domains that are considered to be affected early and characteristically in Alzheimer's disease ([Scarapicchia et al.](#),

2018; Kueper et al., 2018). It is important to note that higher scores are associated with more serious cognitive deficiency. To study how functional connectivity in the brain varies with the total cognitive score for subjects at different ages, we applied the CORE models. It is known that age affects both functional connectivity in the brain and total cognitive score so that the relation of cognitive deficits with brain connectivity likely changes with age.

We implemented a time-varying or concurrent regression framework with the Pearson correlation matrices in (26) as time-varying object responses, residing in the metric space of correlation matrices equipped with the Frobenius norm, and total cognitive scores as real-valued covariates, changing with time (age in years). Specifically, we fitted the Nonparametric CORE in (11) separately for the AD and CN subjects over different output points for age t_0 and total cognitive score x_0 . The bandwidths in the local fits for both the age and total cognitive score directions were chosen satisfying a leave-one-out cross validation criterion with a bivariate Normal kernel function, which led to the bandwidths in Table 1.

	AD	CN
h_1	4.95	3.64
h_2	5.78	2.43

Table 1: Bandwidths used in the Nonparametric CORE model for the AD and CN subjects, here h_1 is the bandwidth for age and h_2 for total cognitive score.

We fitted the proposed model at the $x_0 = 10\%$, 50% , and 90% quantile values in the total cognitive score direction, where higher total score means larger cognitive impairment. We find that for higher scores and thus increased cognitive impairment, the overall magnitude of the absolute values of the pairwise correlations is smaller, and interestingly there are fewer negative correlations. These effects are more pronounced at older age.

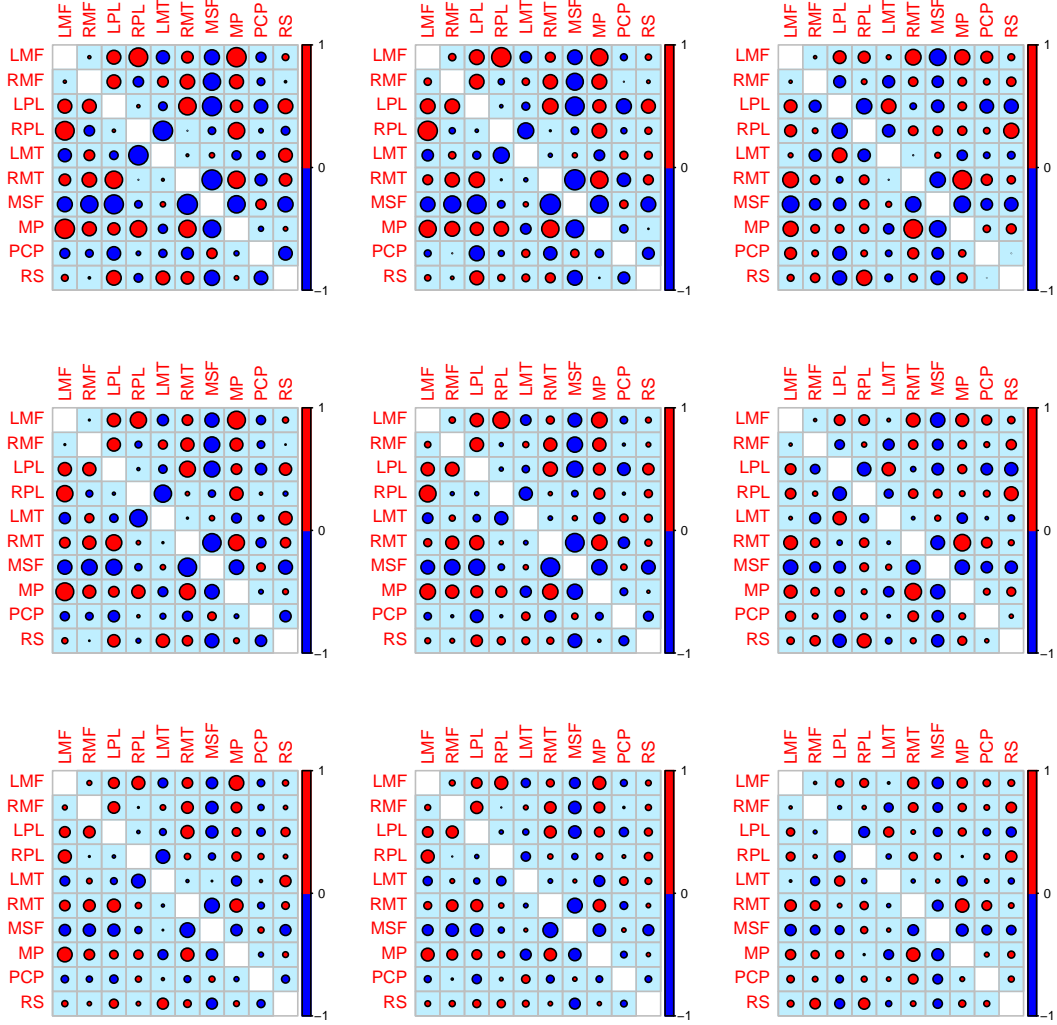


Figure A2: Estimated correlation matrix for the AD subjects fitted locally using Non-parametric CORE in (11). The top, middle and bottom rows show, respectively, the fitted correlation matrices at 10%, 50%, and 90% quantiles of age. For each such age quantile, the columns (from left to right) depict the estimated correlation structure at $x_0 = 10\%$, 50%, and 90% quantiles of total cognitive score respectively. Positive (negative) values are drawn in red (blue) and larger circles correspond to larger absolute values. The figure illustrates the dependence of functional connectivity on total cognitive score, modulated by age.

Perhaps the most interesting finding from the fit (Figure A2) is the variation of Negative Functional Connectivity (NFC) for the AD subjects (Zhou et al., 2010; Brier et al., 2012; Wang et al., 2007). The positive pairwise correlations between the functional

hubs, though reduced in magnitude, has a higher count when moving from a lower to a higher value in the total cognitive score direction. However, in the same context, the negative correlations diminish much more ostensibly in number and magnitude. Thus an increasing reduction in the negative connectivity can be associated with higher cognitive impairment, and hence an increased cognitive impairment, in the AD subjects.

Also, the association between the functional connectivity and total cognitive score is modulated by age, in the sense that at lower ages the association between cognitive impairment and reduction in Negative Functional Connectivity is weaker than it is at higher ages. Table 2 shows the difference, measured from the fits in Figure A2, between the total magnitude of the positive and the negative pairwise correlations, the latter being subtracted from the former. At each fixed age t_0 , the difference decreases with an increased value of the total cognitive score x_0 , where the absolute values of the difference depend on age. A similar concurrent or time-varying pattern in the estimated correlation matrices is also present for the CN subjects (Figure A10 Appendix A6).

	Lower score ($x_0 = 10\%$ quantile of total score)	Median score ($x_0 = 50\%$ quantile of total score)	Higher score ($x_0 = 90\%$ quantile of total score)
Lower age ($t_0 = 10\%$ quantile of age)	10.23	9.16	7.12
Median age ($t_0 = 50\%$ quantile of age)	9.55	7.96	7.92
Higher age ($t_0 = 90\%$ quantile of age)	9.27	7.70	7.25

Table 2: Difference in the total magnitude of positive correlations and the total magnitude of total negative correlation present in the estimated matrices in Figure A2 at varying output points of total cognitive score and age.

We also fitted the Partially Global CORE, as defined in (17), to the same data

and compared their performance, where the effect of total cognitive scores on the age-dependent functional connectivity correlation matrices is modeled as linear and the effect of age as nonparametric. To this end, the model was fitted separately for the AD and the CN subjects. The bandwidth parameter in the “age” direction was again chosen using a leave-one-out cross validation criterion and a Gaussian kernel was used. For the AD and CN subjects the optimal bandwidths were found to be 4.12 and 3.22, respectively. We present the fits corresponding to the AD subjects over a range of output points in Figure A3. We find a very similar pattern for the fitted correlation. The positive correlations increase in magnitude and quantity with increasing total cognitive score and age, while the curious changes in the Negative Functional Correlations are again noted.

To investigate the comparative goodness-of-fit of the two models, we computed the average deviation of the fitted from the observed correlation matrices over the age interval $[55, 90]$,

$$\text{MSE}_{\oplus}(t) := d_F^2(M_{\oplus}(t), \hat{M}_{\oplus}(t)), \quad (27)$$

$M_{\oplus}(t)$ and $\hat{M}_{\oplus}(t)$ being the observed and fitted connectivity matrices, respectively, at age $t \in [55, 90]$ and $d_F(\cdot, \cdot)$ the Frobenius distance between two correlation matrices. Deviation (27) is displayed in Figure A4 for both the Nonparametric and Partially Global CORE models. The Partially Global model seems to fit the data better, which could indicate that the linear constraint for the impact of total cognitive score imposed in the Partially Global Core model is likely satisfied. The integrated deviance $\int_{\mathcal{T}} \text{MSE}_{\oplus}(t) dt$ is 0.0570 for the Nonparametric CORE and 0.0494 for the Partially CORE.

We further look into the out-of-sample prediction performance of the two methods for the AD subjects and CN subjects separately. For this, we first randomly split the dataset into a training set with sample size n_{train} and a test set with the remaining n_{test} subjects. We then take the fitted objects obtained from the training set, and predict the

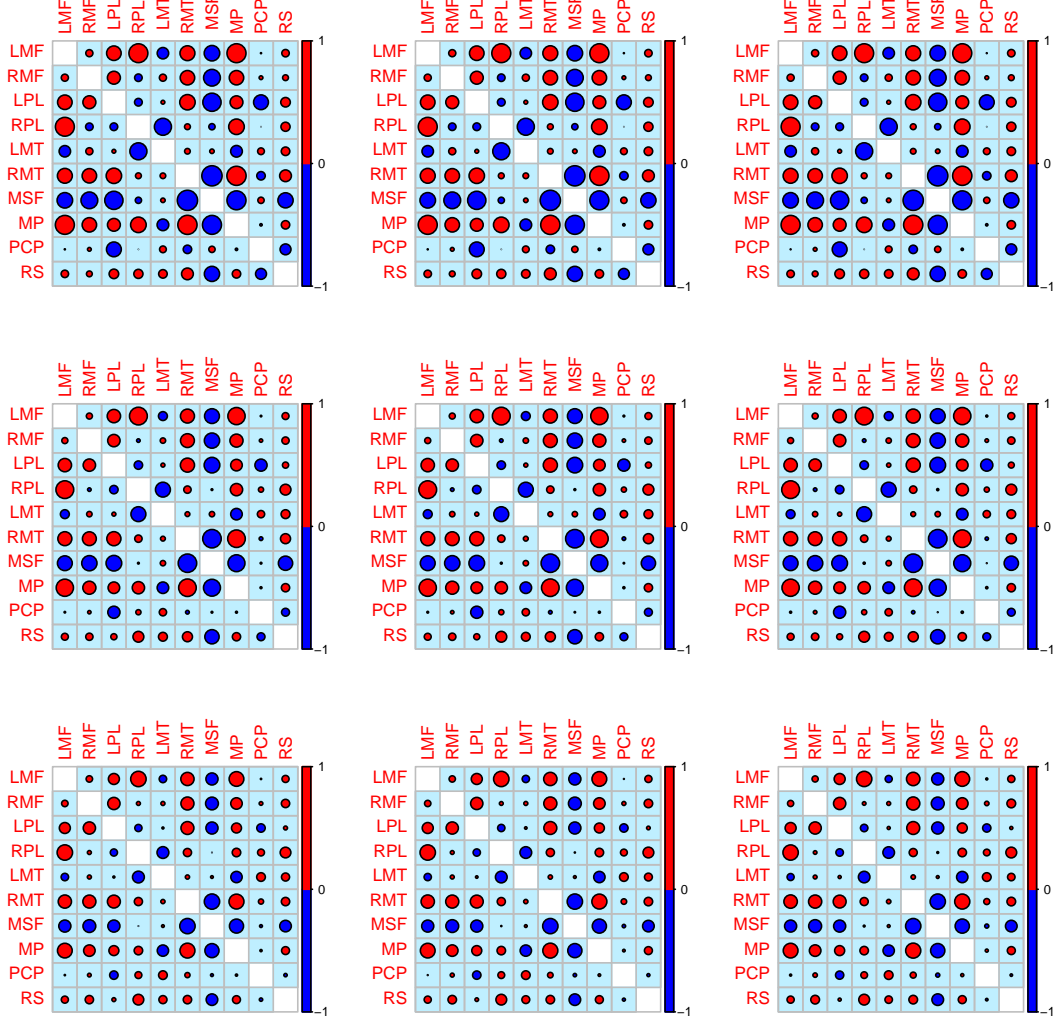


Figure A3: Estimated correlation matrix for the AD subjects fitted locally using Partially Global CORE in (17). The top, middle and bottom rows show, respectively, the fitted correlation matrices at 10%, 50%, and 90% quantiles of age. For each such age quantile, the columns (from left to right) depict the estimated correlation structure at $x_0 = 10\%$, 50%, and 90% quantiles of total cognitive score respectively. Positive (negative) values are drawn in red (blue) and larger circles correspond to larger absolute values. The figure illustrates the dependence of functional connectivity on total cognitive score, modulated by age.

responses in the test set using the covariates present in the test set. As a measure of the

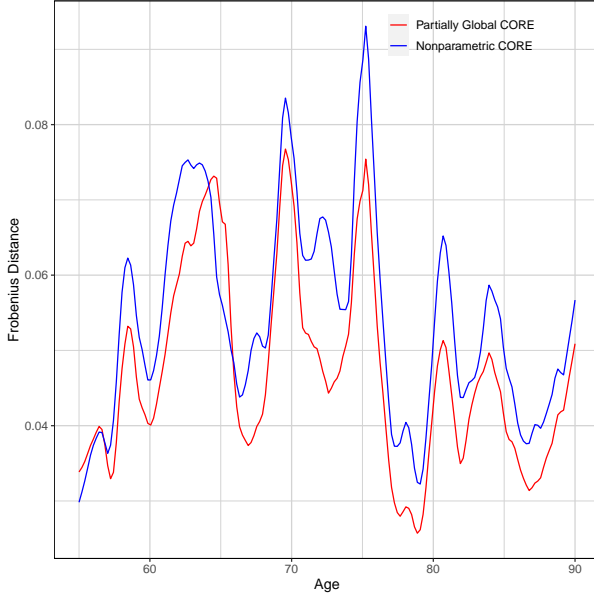


Figure A4: Comparison of fits for the two CORE models. The figure shows the Frobenius distances between the fitted and the observed correlation matrices across age for the AD subjects using the Nonparametric CORE model (blue) and the Partially Global CORE model (red) are illustrated.

efficacy of the fitted model, we compute root mean squared prediction error as

$$\text{RMPE} = \left[\frac{1}{n_{\text{test}}} \sum_{i=1}^{n_{\text{test}}} n_i^{-1} \sum_{l=1}^{n_i} d_F^2 \left(Y_{il}^{\text{test}}, \hat{l}_{\oplus}(X_{il}, T_{il}) \right) \right]^{-1/2}, \quad (28)$$

where Y_{il}^{test} and $\hat{l}_{\oplus}(X_{il}, T_{il})$ denote, respectively, the i^{th} actual and predicted responses in the test set, evaluated at age T_{il} and total cognitive score X_{il} . We repeat this process 1000 times, and compute RMPE for each split for the AD and CN subjects separately (See Table 3). We observe that the out-of-sample predictions errors are quite low for both the AD and CN subjects. In fact they are in the ballpark of the in-sample-prediction error, calculated as the average distance between the observed training sample and the predicted objects based on the covariates in the training sets, which supports the proposed CORE models. The Nonparametric model shows a better predictive performance than the Partially Global CORE.

	n_{train}	n_{test}	nonparametric CORE	Partially Global CORE)
AD	52	26	0.306	0.322
CN	271	100	0.151	0.167

Table 3: Average Root Mean Prediction Error (RMPE) over 1000 repetitions for the AD and CN subjects, as obtained from the local fits of the Nonparametric and Partially Global CORE models. Here, n_{train} and n_{test} denote the sample sizes for the splitted training and testing datasets respectively.

To confirm the group differences in the time-varying structure of the correlation matrices we further conduct a permutation test. To test the null hypothesis that, for varying age and total cognitive score values, the AD and CN subjects have the same conditional correlation matrix objects, we use the test statistic

$$\int S(x, t) dx dt = \int \|\hat{\Sigma}^{\text{AD}}(x, t) - \hat{\Sigma}^{\text{CN}}(x, t)\|_F dx dt,$$

where $\hat{\Sigma}^{\text{AD}}(x, t)$ and $\hat{\Sigma}^{\text{CN}}(x, t)$ denote the estimated correlation matrix objects at total cognitive score x and age t , for the AD and CN subjects respectively, with $x \in [5, 70]$ and varying age $t \in [55, 90]$ and $\|\cdot, \cdot\|_F$ is the Frobenius norm between two matrix objects.

All the observations are pooled, and the test statistic calculated for every possible way of dividing the pooled values into two groups of size 174 and 694. The set of these calculated test statistic values is the exact distribution of possible differences under the null hypothesis. The p-value of the test is calculated as the proportion of sampled permutations where the computed test-statistic value is more than or equal to the test statistic value obtained from the observed sample. Using 10^6 permutation samples, and the estimation methods being the Nonparametric CORE and Partially Global CORE, the p-values are found to be 0.009 and 0.002 , respectively. Thus both the methods are able to detect a significant difference in the functional connectivity between the AD and CN subjects, providing evidence that the CORE model is useful to differentiate these groups. A further look into the time-varying regression fits for those connectivity hubs that show

a change in the magnitude of the correlations across the AD and CN subjects (Figure A12 in Appendix A6) also indicates differences between the AD and CN subjects.

7 CONCLUDING REMARKS

The proposed Concurrent Object Regression (CORE) is useful for the regression analysis of random objects, where it complements Fréchet regression, by extending the notion of conditional Fréchet means further to a concurrent or varying coefficient framework. We provide theoretical justifications including rates of pointwise convergence for both global and local versions of the CORE model, and a uniform convergence result for the global part. For the special case of Euclidean objects the rates of convergence correspond to the known optimal rates. The rate of convergence for the Nonparametric CORE model is intrinsically connected to an inherent manifold structure of the predictor space.

Analogously to local regression, the nonparametric estimators will suffer from the curse of dimensionality if the predictor space is of higher dimension than $p = 2$ or $p = 3$. This calls for future research in dimension reduction in the predictor space.

A feature of interest is that we do not require observing the complete stochastic processes $\{(X(t), Y(t)) : t \in \mathcal{T}\}$ but only need samples taken at random predictor times, and our methods can be adapted for sparse and longitudinal predictors.

8 ACKNOWLEDGEMENTS

Data collection and sharing for this project was funded by the Alzheimer’s Disease Neuroimaging Initiative (ADNI) (National Institutes of Health Grant U01 AG024904) and DOD ADNI (Department of Defense award number W81XWH-12-2-0012). ADNI is funded by the National Institute on Aging, the National Institute of Biomedical Imaging and Bioengineering, and through generous contributions from the following: AbbVie, Alzheimer’s Association; Alzheimer’s Drug Discovery Foundation; Araclon Biotech; BioClinica, Inc.; Biogen; Bristol-Myers Squibb Company; CereSpir, Inc.; Cogstate; Eisai Inc.; Elan Pharmaceuticals, Inc.; Eli Lilly and Company; EuroImmun; F. Hoffmann-La Roche

Ltd and its affiliated company Genentech, Inc.; Fujirebio; GE Healthcare; IXICO Ltd.; Janssen Alzheimer Immunotherapy Research & Development, LLC.; Johnson & Johnson Pharmaceutical Research & Development LLC.; Lumosity; Lundbeck; Merck & Co., Inc.; Meso Scale Diagnostics, LLC.; NeuroRx Research; Neurotrack Technologies; Novartis Pharmaceuticals Corporation; Pfizer Inc.; Piramal Imaging; Servier; Takeda Pharmaceutical Company; and Transition Therapeutics. The Canadian Institutes of Health Research is providing funds to support ADNI clinical sites in Canada. Private sector contributions are facilitated by the Foundation for the National Institutes of Health (www.fnih.org). The grantee organization is the Northern California Institute for Research and Education, and the study is coordinated by the Alzheimer's Therapeutic Research Institute at the University of Southern California. ADNI data are disseminated by the Laboratory for Neuro Imaging at the University of Southern California.

REFERENCES

Afsari, B. (2011). Riemannian L^p center of mass: existence, uniqueness, and convexity. *Proceedings of the American Mathematical Society*, 139(2):655–673.

Allen, E., Damaraju, E., Plis, S., Erhardt, E., Eichele, T., and Calhoun, V. (2014). Tracking whole-brain connectivity dynamics in the resting state. *Cerebral Cortex*, 24(3):663–676.

Arsigny, V., Fillard, P., Pennec, X., and Ayache, N. (2007). Geometric means in a novel vector space structure on symmetric positive-definite matrices. *SIAM journal on matrix analysis and applications*, 29(1):328–347.

Bhattacharya, R. and Patrangenaru, V. (2005). Large sample theory of intrinsic and extrinsic sample means on manifolds: Ii. *Annals of statistics*, pages 1225–1259.

Bhattacharya, R., Patrangenaru, V., et al. (2003). Large sample theory of intrinsic and extrinsic sample means on manifolds. *The Annals of Statistics*, 31(1):1–29.

Brier, M. R., Thomas, J. B., Snyder, A. Z., Benzinger, T. L., Zhang, D., Raichle, M. E., Holtzman, D. M., Morris, J. C., and Ances, B. M. (2012). Loss of intranetwork and internetwork resting state functional connections with Alzheimer's disease progression. *Journal of Neuroscience*, 32(26):8890–8899.

Buckner, R. L., Sepulcre, J., Talukdar, T., Krienen, F. M., Liu, H., Hedden, T., Andrews-Hanna, J. R., Sperling, R. A., and Johnson, K. A. (2009). Cortical hubs revealed by intrinsic functional connectivity: mapping, assessment of stability, and relation to Alzheimer's disease. *Journal of Neuroscience*, 29(6):1860–1873.

Chiang, C.-T., Rice, J. A., and Wu, C. O. (2001). Smoothing spline estimation for varying coefficient models with repeatedly measured dependent variables. *Journal of the American Statistical Association*, 96(454):605–619.

Cleveland, W. S., Grosse, E., and Shyu, W. M. (2017). Local regression models. In *Statistical models in S*, pages 309–376. Routledge.

Cornea, E., Zhu, H., Kim, P., and Ibrahim, J. G. (2017). Regression models on Riemannian symmetric spaces. *Journal of the Royal Statistical Society Series B*, 79(2):463–482.

Damoiseaux, J. S., Prater, K. E., Miller, B. L., and Greicius, M. D. (2012). Functional connectivity tracks clinical deterioration in Alzheimer’s disease. *Neurobiology of Aging*, 33(4):828–e19.

Dryden, I. L., Koloydenko, A., Zhou, D., et al. (2009). Non-euclidean statistics for covariance matrices, with applications to diffusion tensor imaging. *The Annals of Applied Statistics*, 3(3):1102–1123.

Dryden, I. L., Kolydenko, A., Zhou, D., and Li, B. (2010). Non-euclidean statistical analysis of covariance matrices and diffusion tensors. *arXiv preprint arXiv:1010.3955*.

Eubank, R., Huang, C., Maldonado, Y. M., Wang, N., Wang, S., and Buchanan, R. (2004). Smoothing spline estimation in varying-coefficient models. *Journal of the Royal Statistical Society: Series B (Statistical Methodology)*, 66(3):653–667.

Fan, J. and Zhang, J.-T. (2000). Two-step estimation of functional linear models with applications to longitudinal data. *Journal of the Royal Statistical Society: Series B (Statistical Methodology)*, 62(2):303–322.

Fan, J. and Zhang, W. (1999). Statistical estimation in varying coefficient models. *The Annals of Statistics*, 27(5):1491–1518.

Fan, J. and Zhang, W. (2008). Statistical methods with varying coefficient models. *Statistics and its Interface*, 1(1):179.

Ferreira, L. R. K. and Busatto, G. F. (2013). Resting-state functional connectivity in normal brain aging. *Neuroscience & Biobehavioral Reviews*, 37:384–400.

Fréchet, M. R. (1948). Les éléments aléatoires de nature quelconque dans un espace distancié. *Annales de l’institut Henri Poincaré*, 10(4):215–310.

Hastie, T. and Tibshirani, R. (1993). Varying-coefficient models. *Journal of the Royal Statistical Society. Series B (Methodological)*, 55(4):757–796.

Hoover, D. R., Rice, J. A., Wu, C. O., and Yang, L.-P. (1998). Nonparametric smoothing estimates of time-varying coefficient models with longitudinal data. *Biometrika*, 85(4):809–822.

Horváth, L. and Kokoszka, P. (2012). *Inference for functional data with applications*, volume 200. Springer Science & Business Media.

Huang, J. Z., Wu, C. O., and Zhou, L. (2002). Varying-coefficient models and basis function approximations for the analysis of repeated measurements. *Biometrika*, 89(1):111–128.

Kloeckner, B. (2010). A geometric study of wasserstein spaces: Euclidean spaces. *Annali della Scuola Normale Superiore di Pisa-Classe di Scienze*, 9(2):297–323.

Kueper, J. K., Speechley, M., and Montero-Odasso, M. (2018). The Alzheimer’s disease assessment scale—cognitive subscale (adas-cog): modifications and responsiveness in pre-dementia populations. a narrative review. *Journal of Alzheimer’s Disease*, 63(2):423–444.

Lin, Z. (2019). Riemannian geometry of symmetric positive definite matrices via cholesky decomposition. *SIAM Journal on Matrix Analysis and Applications*, 40(4):1353–1370.

Maity, A. (2017). Nonparametric functional concurrent regression models. *Wiley Interdisciplinary Reviews: Computational Statistics*, 9(2):e1394.

Manrique, T., Crambes, C., and Hilgert, N. (2018). Ridge regression for the functional concurrent model. *Electronic Journal of Statistics*, 12(1):985–1018.

Marron, J. S. and Alonso, A. M. (2014). Overview of object oriented data analysis. *Biometrical Journal*, 56(5):732–753.

Moakher, M. (2005). A differential geometric approach to the geometric mean of symmetric positive-definite matrices. *SIAM Journal on Matrix Analysis and Applications*, 26(3):735–747.

Müller, H.-G. (2016). Peter Hall, functional data analysis and random objects. *The Annals of Statistics*, 44(5):1867–1887.

Patrangenaru, V. and Ellingson, L. (2015). *Nonparametric statistics on manifolds and their applications to object data analysis*. CRC Press.

Pennec, X. et al. (2018). Barycentric subspace analysis on manifolds. *The Annals of Statistics*, 46(6A):2711–2746.

Pennec, X., Fillard, P., and Ayache, N. (2006). A riemannian framework for tensor computing. *International Journal of computer vision*, 66(1):41–66.

Petersen, A. and Müller, H.-G. (2019). Fréchet regression for random objects with euclidean predictors. *The Annals of Statistics*, 47(2):691–719.

Pigoli, D., Aston, J. A., Dryden, I. L., and Secchi, P. (2014). Distances and inference for covariance operators. *Biometrika*, 101(2):409–422.

Ramsay, J. O. and Silverman, B. W. (2005). *Functional Data Analysis*. Springer Series in Statistics. Springer, 2nd edition.

Ramsay, J. O. and Silverman, B. W. (2007). *Applied Functional Data Analysis: Methods and Case Studies*. Springer.

Scarapicchia, V., Mazerolle, E. L., Fisk, J. D., Ritchie, L. J., and Gawryluk, J. R. (2018). Resting state bold variability in Alzheimer’s disease: A marker of cognitive decline or cerebrovascular status? *Frontiers in Aging Neuroscience*, 10:39.

Shi, J. Q., Wang, B., Murray-Smith, R., and Titterington, D. M. (2007). Gaussian process functional regression modeling for batch data. *Biometrics*, 63(3):714–723.

Sturm, K.-T. (2003). Probability measures on metric spaces of nonpositive. *Heat Kernels and Analysis on Manifolds, Graphs, and Metric Spaces: Lecture Notes from a Quarter Program on Heat Kernels, Random Walks, and Analysis on Manifolds and Graphs: April 16-July 13, 2002, Emile Borel Centre of the Henri Poincaré Institute, Paris, France*, 338:357.

Van Der Vaart, A. and Wellner, J. (2000). *Weak Convergence and Empirical Processes: With Applications to Statistics (Springer Series in Statistics)*. Springer, corrected edition.

Verzelen, N., Tao, W., and Mueller, H.-G. (2012). Inferring stochastic dynamics from functional data. *Biometrika*, 99(3):533–550.

Wang, B. and Shi, J. Q. (2014). Generalized Gaussian process regression model for non-Gaussian functional data. *Journal of the American Statistical Association*, 109(507):1123–1133.

Wang, J.-L., Chiou, J.-M., and Müller, H.-G. (2016). Functional data analysis. *Annual Review of Statistics and its Application*, 3:257–295.

Wang, K., Liang, M., Wang, L., Tian, L., Zhang, X., Li, K., and Jiang, T. (2007). Altered functional connectivity in early Alzheimer’s disease: A resting-state fMRI study. *Human Brain Mapping*, 28(10):967–978.

Wang, L., Li, H., and Huang, J. Z. (2008). Variable selection in nonparametric varying-coefficient models for analysis of repeated measurements. *Journal of the American Statistical Association*, 103(484):1556–1569.

Wu, C. O. and Chiang, C.-T. (2000). Kernel smoothing on varying coefficient models with longitudinal dependent variable. *Statistica Sinica*, pages 433–456.

Yuan, Y., Zhu, H., Styner, M., Gilmore, J. H., and Marron, J. S. (2013). Varying coefficient model for modeling diffusion tensors along white matter tracts. *The Annals of Applied Statistics*, 7(1):102–125.

Zhang, H.-Y., Wang, S.-J., Liu, B., Ma, Z.-L., Yang, M., Zhang, Z.-J., and Teng, G.-J. (2010). Resting brain connectivity: changes during the progress of Alzheimer disease. *Radiology*, 256(2):598–606.

Zhang, J., Clayton, M. K., and Townsend, P. A. (2011). Functional concurrent linear regression model for spatial images. *Journal of Agricultural, Biological, and Environmental Statistics*, 16(1):105–130.

Zhou, D., Dryden, I. L., Koloydenko, A. A., Audenaert, K. M., and Bai, L. (2016). Regularisation, interpolation and visualisation of diffusion tensor images using non-euclidean statistics. *Journal of Applied Statistics*, 43(5):943–978.

Zhou, J., Greicius, M. D., Gennatas, E. D., Growdon, M. E., Jang, J. Y., Rabinovici, G. D., Kramer, J. H., Weiner, M., Miller, B. L., and Seeley, W. W. (2010). Divergent network connectivity changes in behavioural variant frontotemporal dementia and Alzheimer’s disease. *Brain*, 133(5):1352–1367.

Zhu, H., Chen, Y., Ibrahim, J. G., Li, Y., Hall, C., and Lin, W. (2009). Intrinsic regression models for positive-definite matrices with applications to diffusion tensor imaging. *Journal of the American Statistical Association*, 104(487):1203–1212.

Zhu, H., Styner, M., Li, Y., Kong, L., Shi, Y., Lin, W., Coe, C., and Gilmore, J. H. (2010). Multivariate varying coefficient models for DTI tract statistics. In *International Conference on Medical Image Computing and Computer-Assisted Intervention*, pages 690–697. Springer.

Sentürk, D. and Müller, H.-G. (2010). Functional varying coefficient models for longitudinal data. *Journal of the American Statistical Association*, 105(491):1256–1264.

Sentürk, D. and Nguyen, D. V. (2011). Varying coefficient models for sparse noise-contaminated longitudinal data. *Statistica Sinica*, 21(4):1831–1856.

A APPENDIX

A1 Proofs for Section 3

Recall the definition of the auxiliary parameters introduced in (7),

$$\begin{aligned}\mu_{jk} &= E \left(K_{h_1, h_2}(X - x_0, T - t_0)(X - x_0)^j(T - t_0)^k \right), \text{ and} \\ \tau_{jk}(y) &:= E \left(K_{h_1, h_2}(X - x_0, T - t_0)(X - x_0)^j(T - t_0)^k | Y = y \right) \text{ for all } j, k = 0, 1, 2.\end{aligned}$$

Lemma 1. *Under assumptions (A1), (A2),*

$$\begin{aligned}\mu_{jk} &= h^{j+k} \left[f_{X,T}(x_0, t_0) K_{jk} + h K_{(j+1)k} \left(\frac{\partial}{\partial x} f_{X,T}(x, t) \right) \Big|_{(x_0, t_0)} \right. \\ &\quad \left. + h K_{j(k+1)} \left(\frac{\partial}{\partial t} f_{X,T}(x, t) \right) \Big|_{(x_0, t_0)} + O(h^2) \right], \\ \tau_{jk}(y) &= h^{j+k} \left[f_{(X,T)|Y}(x_0, t_0, y) K_{jk} + h K_{(j+1)k} \left(\frac{\partial}{\partial x} f_{(X,T)|Y}(x, t, y) \right) \Big|_{(x_0, t_0)} \right. \\ &\quad \left. + h K_{j(k+1)} \left(\frac{\partial}{\partial t} f_{(X,T)|Y}(x, t, y) \right) \Big|_{(x_0, t_0)} + O(h^2) \right],\end{aligned}$$

where the $O(h^2)$ terms are uniform over $y \in \Omega$.

Proof. It is a straightforward application of a Taylor expansion around the neighborhood of the point (x_0, t_0) on the densities, making use of the assumptions, \square

Recall,

$$\sigma_0^2 = (\mu_{00}\mu_{20}\mu_{02} - \mu_{00}\mu_{11}^2 - \mu_{10}^2\mu_{02} - \mu_{01}^2\mu_{20} + 2\mu_{01}\mu_{10}\mu_{11}).$$

From Lemma 1, it follows that $\sigma_0^2 = h^4 [M f_{X,T}^3(x_0, t_0) + O(h)]$ for some constant $M > 0$.

Lemma 2. *Under assumptions (A1)-(A7) and additionally assuming that,*

$$\sup_{x,t,y} |f''_{(X,T)|Y=y}(x,t,y)| < \infty,$$

$$\tilde{L}_\oplus(\omega, x_0, t_0) = M_\oplus(\omega, x_0, t_0) + O(h^2).$$

Proof. The proof follows a similar line of argument as in the proof of Theorem 3 in Petersen and Müller (2019) with some necessary changes due to the differences in the setup. We first establish that

$$\frac{dF_{Y|(X,T)}(y, x, t)}{dF_Y(y)} = \frac{f_{(X,T)|Y}(x, t, y)}{f_{(X,T)(x,t)}} \quad \text{for all } (x, t) \text{ such that } f_{X,T}(x, t) > 0. \quad (29)$$

For any open set $U \subset \Omega$ define,

$$a(x, t) := \int_U \frac{f_{(X,T)|Y}(x, t, y)}{f_{(X,T)}(x, t)} dF_Y(y); \quad b(x, t) = \int_U dF_{Y|(X,T)}(y, x, t),$$

and observe that by assumption (A3), both $a(\cdot, \cdot)$ and $b(\cdot, \cdot)$ are continuous functions of (x, t) . Then for any measurable set A in the Borel sigma algebra on \mathbb{R}^2 ,

$$\begin{aligned} \int_A a(x, t) f_{(X,T)}(x, t) dx dt &= \int_U \left(\int_A f_{(X,T)|Y}(x, t, y) dx dt \right) dF_Y(y) \\ &= \int_A \left(\int_U dF_{Y|(X,T)}(y, x, t) \right) f_{(X,T)}(x, t) dx dt = \int_A b(x, t) f_{(X,T)}(x, t) dx dt. \end{aligned}$$

The fact that this holds for any measurable set A then implies (29). Next observing that,

$$s^L(X, x_0, T, t_0, h_1, h_2) = K_{h_1, h_2}(X - x_0, T - t_0) [\nu_1 + \nu_2(X - x_0) + \nu_3(T - t_0)].$$

we have,

$$\begin{aligned}
& \int s^L(x, x_0, t, t_0, h) dF_{(X,T)|Y}(x, t, y) \\
&= \frac{1}{\sigma_0^2} \left[(\mu_{20}\mu_{02} - \mu_{11}^2) \tau_{00}(y) + (\mu_{01}\mu_{11} - \mu_{02}\mu_{10}) \tau_{10}(y) + (\mu_{10}\mu_{11} - \mu_{20}\mu_{01}) \tau_{01}(y) \right] \\
&= \frac{f_{(X,T)|Y}(x, t, y)}{f_{(X,T)}(x, t)} + O(h^2),
\end{aligned}$$

where the error term is uniform over $y \in \Omega$. Finally,

$$\begin{aligned}
\tilde{L}_\oplus(\omega, x_0, t_0) &= \int d^2(y, \omega) s^L(x, x_0, t, t_0, h) dF(x, t, y) \\
&= \int d^2(y, \omega) \left(\frac{f_{(X,T)|Y}(x, t, y)}{f_{(X,T)}(x, t)} + O(h^2) \right) dF_Y(y) \\
&= \int d^2(y, \omega) \left(\frac{dF_{Y|(X,T)}(y, x, t)}{dF_Y(y)} + O(h^2) \right) dF_Y(y) \\
&= \int d^2(y, \omega) dF_{Y|(X,T)}(y, x, t) + O(h^2) = M_\oplus(\omega, x_0, t_0) + O(h^2),
\end{aligned}$$

where, again, the error term is uniform over $\omega \in \Omega$. Thus the intermediate objective function in (11) is a smoothed version of the true objective function in (3). \square

Proof of Proposition 1. Assumptions (A3), (A4) regarding the existence and uniqueness of the minimizer $\tilde{l}_\oplus(x_0, t_0)$ and the well-separatedness of the objective functions at the minimizer imply $d(m_\oplus(x_0, t_0), \tilde{l}_\oplus(x_0, t_0)) = o(1)$ as $h = h_n \rightarrow 0$. The $O(h^2)$ rate of convergence follows by adapting a similar proof technique as in Theorem 3 of Petersen and Müller (2019). \square

Lemma 3. *Under assumptions (A8), (A9),*

$$\hat{\mu}_{jk} = \mu_{jk} + O_p \left[(h^{2j+2k-1} n^{-1})^{\frac{1}{2}} \right].$$

Proof. We provide the proof for the case $p = 1$ only. The case $p > 1$ is based on essentially the same but more tedious arguments. The proof exploits the manifold structure of the predictor space as described before. The fact that $E(\hat{\mu}_{jk}) = \mu_{jk}$ follows immediately. For calculating $\text{Var}(\hat{\mu}_{jk})$, first consider the case $n_i = 1$ for $i = 1, \dots, n$. Writing

$$\Psi_{il} = K_h(X_{il} - x_0, T_{il} - t_0) (X_{il} - x_0)^j (T_{il} - t_0)^k,$$

$$\begin{aligned} \text{Var}(\Psi_{il}) &\leq E(\Psi_{il}^2) = E\left(K_h^2(X_{il} - x_0, T_{il} - t_0) (X_{il} - x_0)^{2j} (T_{il} - t_0)^{2k}\right) \\ &= E\left(K_h^2(X_{il} - x_0, T_{il} - t_0) (X_{il} - x_0)^{2j} (T_{il} - t_0)^{2k} \mathbf{1}\left((X_{il}, T_{il}) \in \mathcal{B}_h^{(2)}(t_0, x_0)\right)\right) \\ &\quad + E\left(K_h^2(X_{il} - x_0, T_{il} - t_0) (X_{il} - x_0)^j (T_{il} - t_0)^k \mathbf{1}\left((X_{il}, T_{il}) \notin \mathcal{B}_h^{(2)}(t_0, x_0)\right)\right) \\ &\leq \int \frac{1}{h^4} K^2\left(\frac{x - x_0}{h}, \frac{t - t_0}{h}\right) h^{2j} h^{2k} f_{(X,T)}(x, t) \mathbf{1}\left((x, t) \in \mathcal{B}_h^{(2)}(t_0, x_0)\right) dx dt \\ &\quad + o_P(h^{1+2j+2k}) \\ &= h^{2j+2k-2} \int K^2(u, v) \left[f_{X,T}(x_0, t_0) + h \frac{\partial}{\partial u} f_{X,T}(u, v) \Big|_{(x_0, t_0)} + h \frac{\partial}{\partial v} f_{X,T}(u, v) \Big|_{(x_0, t_0)} \right. \\ &\quad \left. + O(h^2) \right] \mathbf{1}\left((u, v) \in \mathcal{B}_h^{(2)}(0, 0)\right) f_{X,T}(u, v) du dv + o_P(h^{1+2j+2k}) \\ &\leq h^{2j+2k-2} A_1 E\left(\mathbf{1}\left((X, T) \in \mathcal{B}_h^{(2)}(x_0, t_0)\right)\right) + o_P(h^{1+2j+2k}), \end{aligned}$$

for some positive constant A_1 . Note that the Ψ_{il} is independent across i . By (A9) we obtain with some proportionality constant $c_{t_0} > 0$ that

$$\begin{aligned} \text{Var}(\hat{\mu}_{jk}) &= \text{Var}\left(\frac{1}{n} \sum_{i=1}^n \Psi_{il}\right) = \frac{1}{n^2} \sum_{i=1}^n \text{Var}(\Psi_{il}) \leq \frac{1}{n^2} \sum_{i=1}^n E(\Psi_{il}^2) \\ &= \frac{1}{n^2} \left[\sum_{i=1}^n A_1 h^{2j+2k-2} E\left(\mathbf{1}\left((X, T) \in \mathcal{B}_h^{(2)}(x_0, t_0)\right)\right) + o_P(h^{1+2j+2k}) \right] \\ &= \frac{1}{n^2} [h^{2j+2k-2} c A_1 (nh) + o_P(h^{1+2j+2k})] = O(h^{2j+2k-1} n^{-1}). \end{aligned}$$

For the case $n_i \geq 1$ we observe that the Ψ_{il} are not independent anymore, as the covariates are measured $l = 1, \dots, n_i$ times for the same subject. Using the result just derived for the case $n_i = 1$ and applying the Cauchy-Schwarz inequality,

$$\begin{aligned}\text{Var}(\hat{\mu}_{jk}) &= \text{Var}\left[\frac{1}{n} \sum_{i=1}^n \left(\frac{1}{n_i} \sum_{l=1}^{n_i} \Psi_{il}\right)\right] = \frac{1}{n^2} \sum_{i=1}^n \text{Var}\left(\frac{1}{n_i} \sum_{l=1}^{n_i} \Psi_{il}\right) \\ &= \frac{1}{n^2} \sum_{i=1}^n \left[\frac{1}{n_i^2} \sum_{l=1}^{n_i} \sum_{l'=1}^{n_i} \text{cov}(\Psi_{il}, \Psi_{il'}) \right] \leq \frac{1}{n^2} \sum_{i=1}^n \left[\frac{1}{n_i^2} \sum_{l=1}^{n_i} \sum_{l'=1}^{n_i} \sqrt{\text{Var}(\Psi_{il})} \sqrt{\text{Var}(\Psi_{il'})} \right] \\ &= \frac{1}{n^2} \sum_{i=1}^n \left[\frac{1}{n_i^2} \sum_{l=1}^{n_i} \sum_{l'=1}^{n_i} O(h^{2j+2k-1}) \right] = O(h^{2j+2k-1} n^{-1}).\end{aligned}$$

Since $E(\hat{\mu}_{jk}) = \mu_{jk}$ and $\text{Var}(\hat{\mu}_{jk}) = O(h^{2j+2k-1} n^{-1})$, the result follows using Chebyshev's inequality. \square

We note that Lemma 3 also implies that $\hat{\sigma}_0^2 = O_P(n^{-\frac{1}{2}} h^{\frac{7}{2}})$ for the plug in estimator $\hat{\sigma}_0^2$ defined in (13).

Lemma 4. *Under assumptions (A1)- (A9),*

$$d(\tilde{l}_\oplus(x_0, t_0), \hat{l}_\oplus(x_0, t_0)) = o_P(1).$$

Proof. We will first show that $\hat{L}_\oplus - \tilde{L}_\oplus \rightsquigarrow 0$ in $\ell^\infty(\Omega)$, where \rightsquigarrow denotes the weak convergence of a process and $\ell^\infty(\Omega)$ is the space of bounded functions on Ω . As a consequence of Theorem 1.3.6 of Van Der Vaart and Wellner (2000), this will imply that, $\|\hat{L}_\oplus - \tilde{L}_\oplus\|_\Omega := \sup_{\omega \in \Omega} |\hat{L}_\oplus(\omega) - \tilde{L}_\oplus(\omega)| \xrightarrow{\mathbb{P}} 0$, namely, the estimated objective function \hat{L}_\oplus in (16) converges in probability to the intermediate objective function \tilde{L}_\oplus (3). The Lemma follows using Assumption (A4), recalling Theorem 3.2.3 of Van Der Vaart and Wellner (2000).

Define, $s_{il} := K_h(X_{il} - x_0, T_{il} - t_0) [\nu_1 + \nu_2(X_{il} + \nu_3(T_{il} - t_0))]$. Then,

$$\begin{aligned} \hat{L}_\oplus(\omega) - \tilde{L}_\oplus(\omega) &= \frac{1}{n} \sum_{i=1}^n \left(n_i^{-1} \sum_{l=1}^{n_i} [\hat{s}_{il}(x_0, t_0, h) - s_{il}(x_0, t_0, h)] d^2(Y_{il}, \omega) \right) \\ &\quad + \frac{1}{n} \sum_{i=1}^n \left(n_i^{-1} \sum_{l=1}^{n_i} [s_{il}(x_0, t_0, h) d^2(Y_{il}, \omega) - E(s_{il}(x_0, t_0, h) d^2(Y_{il}, \omega))] \right). \end{aligned} \tag{30}$$

Observe that,

$$\hat{s}_{il}(x_0, t_0, h) - s_{il}(x_0, t_0, h) = K_h(X_{il} - x_0, T_{il} - t_0) \left[W_{1n} + W_{2n}(X_{il} - x_0) + W_{3n}(T_{il} - t_0) \right],$$

$$\text{with } W_{1n} = \hat{\nu}_1 - \nu_1; \quad W_{2n} = \hat{\nu}_2 - \nu_2; \quad W_{3n} = \hat{\nu}_3 - \nu_3.$$

Lemma 1 and Lemma 3 imply that $W_{1n} = O_P((nh)^{-1/2})$, $W_{2n} = O_P((nh^3)^{-1/2})$, $W_{3n} = O_P((nh^3)^{-1/2})$. Since

$$\begin{aligned} E(K_h(X_i(T_l) - x_0, T_l - t_0)(X_i(T_l) - x_0)^j(T_l - t_0)^k d^2(Y_i(T_l), \omega)) &= O(h^{j+k}), \\ E(K_h^2(X_i(T_l) - x_0, T_l - t_0)(X_i(T_l) - x_0)^{2j}(T_l - t_0)^{2k} d^4(Y_i(T_l), \omega)) &= O(h^{2j+2k-1}), \\ E(s_{il}^2(x_0, t_0, h)) &= O(h^{-1}), \end{aligned}$$

it follows that both terms in (30) are $O_P((nh)^{-1/2})$. Thus $\hat{L}_\oplus(\omega) - \tilde{L}_\oplus(\omega) = o_P(1)$ for any $\omega \in \Omega$. Also any finite dimensional distribution converges weakly, that is, for any k , $\hat{L}_\oplus(\omega_1) - \tilde{L}_\oplus(\omega_1), \dots, \hat{L}_\oplus(\omega_k) - \tilde{L}_\oplus(\omega_k) \rightsquigarrow 0$. This result along with the asymptotic equicontinuity of the process $(\hat{L}_\oplus(\omega) - \tilde{L}_\oplus(\omega))_{\omega \in \Omega}$ leads to the desired weak convergence of $(\hat{L}_\oplus - \tilde{L}_\oplus)_{\omega \in \Omega}$ in $\ell^\infty(\Omega)$. It remains to show that for any $\eta > 0$,

$$\limsup_N \mathbb{P} \left(\sup_{d(\omega_1, \omega_2) < \delta} \left| (\hat{L}_\oplus - \tilde{L}_\oplus)(\omega_1) - (\hat{L}_\oplus - \tilde{L}_\oplus)(\omega_2) \right| > \eta \right) \rightarrow 0 \text{ as } \delta \rightarrow 0.$$

For this we observe,

$$E(s_{il}(x_0, t_0, h)) = O(1); \quad E(s_{il}^2(x_0, t_0, h)) = O(h^{-1}); \quad \frac{1}{n} \sum_{i=1}^n n_i^{-1} \sum_{l=1}^{n_i} |\hat{s}_{il}(x_0, t_0, h)| = O_P(1),$$

yielding,

$$|\hat{L}_\oplus(\omega_1) - \hat{L}_\oplus(\omega_2)| \leq 2 \operatorname{diam}(\Omega) d(\omega_1, \omega_2) \left[\frac{1}{n} \sum_{i=1}^n \left(\frac{1}{n_i} \sum_{l=1}^{n_i} |\hat{s}_{il}(x_0, t_0, h)| \right) \right] = O_P(d(\omega_1, \omega_2)),$$

$$|\tilde{L}_\oplus(\omega_1) - \tilde{L}_\oplus(\omega_2)| \leq 2 \operatorname{diam}(\Omega) d(\omega_1, \omega_2) E(|s_{il}(x_0, t_0, h)|) = O(d(\omega_1, \omega_2)).$$

Thus,

$$\sup_{d(\omega_1, \omega_2) < \delta} |(\hat{L}_\oplus - \tilde{L}_\oplus)(\omega_1) - (\hat{L}_\oplus - \tilde{L}_\oplus)(\omega_2)|$$

$$\leq \sup_{d(\omega_1, \omega_2) < \delta} |\hat{L}_\oplus(\omega_1) - \hat{L}_\oplus(\omega_2)| + \sup_{d(\omega_1, \omega_2) < \delta} |\tilde{L}_\oplus(\omega_1) - \tilde{L}_\oplus(\omega_2)| \leq \delta,$$

which verifies asymptotic equicontinuity and hence the weak convergence of $(\hat{L}_\oplus(\omega) - \tilde{L}_\oplus(\omega))_{\omega \in \Omega}$ follows and also the result by assumption (A4).

Using Lemma 3, Lemma 4 and Assumptions (A5) - (A8) then yields Proposition 2, following the same line of argument as in the proof of Theorem 4 in Petersen and Müller (2019), and Theorem 1 is a consequence of combining Propositions 1 and 2 with a triangle inequality. \square

A2 Background for the Partially Global Concurrent Object Regression

Proof. Motivation of deriving (17) for the Euclidean response case. When $(\Omega, d) = (\mathbb{R}, d_E)$, we write $m_\oplus(\cdot, \cdot) = m(\cdot, \cdot)$. Assuming the true relation between the response Y and the predictor X is linear while there is a smooth nonparametric relation in the

T direction, a partially local linear type estimator of the regression model $m(\cdot, \cdot)$ is $\hat{m}(x, t_0) = \hat{a}^T(x - \mu) + \hat{\beta}_0$, where $\mu = E(X|T = t) = E_{X|T}(X)$ for all $t \in \mathcal{T}$ and

$$(\hat{a}, \hat{\beta}_0, \hat{\beta}_1) = \underset{a, \beta_0, \beta_1}{\operatorname{argmin}} \frac{1}{n} \sum_{i=1}^n \left[\frac{1}{n_i} \sum_{l=1}^{n_i} K_h(T_{il} - t_0)(Y_{il} - a^T(x - \mu) - \beta_0 - \beta_1(T_{il} - t_0))^2 \right].$$

We can view this as an M-estimator of an intermediate population model,

$$\tilde{g}(x, t_0) = (a_1^*(x, t_0))^\top(x - \mu) + \beta_0^*(t_0), \text{ where}$$

$$\begin{aligned} & (a_1^*, \beta_0^*, \beta_1^*) \\ &= \underset{a_1, \beta_0, \beta_1}{\operatorname{argmin}} \int \left[\int y dF_{Y|X,T}(y, x, t) - a_1^\top(x - \mu) - \beta_0 - \beta_1(t - t_0) \right]^2 K_h(t - t_0) dF_{X,T}(x, t). \end{aligned}$$

Defining as before the following auxiliary parameters for $j = 0, 1, 2$,

$$\begin{aligned} \mu_{0j} &:= E(K_h(T - t_0)(T - t_0)^j), \quad \Sigma_{2j} := E(K_h(T - t_0)(T - t_0)^j(X - \mu)(X - \mu)^\top), \\ r_{0j} &:= E(K_h(T - t_0)(T - t_0)^j Y), \quad r_{1j} := E(K_h(T - t_0)(T - t_0)^j Y(X - \mu)), \\ \sigma_0^2 &:= \mu_{02}\mu_{00} - \mu_{01}^2. \end{aligned}$$

and solving the minimization problem leads to

$$a_1^* = \Sigma_{20}^{-1} r_{10}, \quad \beta_0^* = \frac{r_{00}\mu_{02} - r_{01}\mu_{01}}{\sigma_0^2}, \quad \beta_1^* = \frac{r_{01}\mu_{00} - r_{00}\mu_{01}}{\sigma_0^2}.$$

Putting the optimal values of the parameters back in the model,

$$\tilde{g}(x, t_0) = a_1^*(x, t_0)(x - \mu) + \beta_0^*(x, t_0) = \int s^G(z, x, t, t_0, h) y dF(y, z, t) = E(s^G(X, x, T, t_0, h) Y),$$

with weight function,

$$s^G(z, x, t, t_0, h) = \underbrace{K_h(t - t_0) \left[(z - \mu)^\top \Sigma_{20}^{-1} (x - \mu) \right]}_{s_1(z, x, t, t_0, h)} + \underbrace{\frac{1}{\sigma_0^2} K_h(t - t_0) (\mu_{02} - (t - t_0)\mu_{01})}_{s_2(t, t_0, h)}.$$

Rewriting the framework as the weighted Fréchet mean w.r.t the Euclidean metric,

$$\tilde{g}(x, t_0) = \operatorname{argmin}_{y \in \mathbb{R}} E(s^G(X, x, T, t_0, h)(Y - y)^2) = \operatorname{argmin}_{y \in \mathbb{R}} E(s^G(X, x, T, t_0, h)d_E^2(Y, y)),$$

where \tilde{g} can be viewed as a smoothed version of the true regression function m with bias $m(x, t_0) - \tilde{g}(x, t_0) = o(1)$. This alternative formulation of the combination of a global and a local regression component thus provides the intuition to define the general population model for metric-space valued random objects as

$$\tilde{g}_\oplus(x, t_0) = \operatorname{argmin}_{\omega \in \Omega} \tilde{G}_\oplus(\omega), \text{ where, } \tilde{G}_\oplus(\omega) := E(s^G(X, x, T, t_0, h)d^2(Y, \omega)).$$

□

A3 Assumptions (B1)-(B6) in Section 4

The following is a list of these assumptions which are required for section 4.

- (B1) The kernel function K is a univariate probability density that is symmetric around zero, with $|K_{0j}^\gamma| = |\int K(u)u^j du| < \infty$ for $j = 1, \dots, 4$ and $\gamma = 0, 1, 2$.
- (B2) The marginal density $f_{(X,T)}(x, t)$ and the conditional density $f_{(X,T)|Y}(x, t, y)$ exist, are twice continuously differentiable as a function of t for all x and all y .
- (B3) The Fréchet means $m_\oplus(x, t_0), \tilde{g}_\oplus(x, t_0), \hat{g}_\oplus(x, t_0)$ exist and are unique.

(B4) For any $\epsilon > 0$,

$$\begin{aligned} & \inf_{d(\omega, m_{\oplus}(x_0, t_0)) > \epsilon} (M_{\oplus}(\omega, x_0, t_0) - M_{\oplus}(m_{\oplus}(x_0, t_0), x_0, t_0)) > 0. \\ & \inf_{d(\omega, \tilde{g}_{\oplus}(x_0, t_0)) > \epsilon} (\tilde{G}_{\oplus}(\omega, x_0, t_0) - \tilde{G}_{\oplus}(\tilde{g}_{\oplus}(x_0, t_0), x_0, t_0)) > 0. \end{aligned}$$

(B5) There exist $\eta_1 > 0, C_1 > 0$, with $d(\omega, m_{\oplus}(x_0, t_0)) < \eta_1$ such that

$$M_{\oplus}(\omega, x_0, t_0) - M_{\oplus}(m_{\oplus}(x_0, t_0), x_0, t_0) \geq C_1 d(\omega, m_{\oplus}(x_0, t_0))^2.$$

(B6) There exist $\eta_2 > 0, C_2 > 0$, with $d(\omega, \tilde{g}_{\oplus}(x_0, t_0)) < \eta_2$ such that

$$\liminf_N \left[\tilde{G}_{\oplus}(\omega, x_0, t_0) - \tilde{G}_{\oplus}(\tilde{g}_{\oplus}(x_0, t_0), x_0, t_0) \right] \geq C_2 d(\omega, \tilde{g}_{\oplus}(x_0, t_0))^2.$$

These assumptions are required to ensure the existence and uniqueness of the Fréchet mean in the population and sample cases and the local curvature of the objective functions near their respective minimums to establish consistency of the Partially Global Concurrent Object Regression (CORE) estimator. Also the relevant entropy conditions are necessary to prove the rate of convergence of the CORE estimator.

For proving the uniform convergence results in the X -direction for any fixed value of t_0 , the following additional conditions are used.

(U1) For almost all x such that $\|x\|_E \leq M$, the Fréchet means $m_{\oplus}(x, t_0), \tilde{g}_{\oplus}(x, t_0), \hat{g}_{\oplus}(x, t_0)$ exist and are unique.

(U2) For any $\epsilon > 0$, $\inf_{\|x\|_E \leq M} \inf_{d(\omega, m_{\oplus}(x, t_0)) > \epsilon} (M_{\oplus}(\omega, x, t_0) - M_{\oplus}(m_{\oplus}(x, t_0), x, t_0)) > 0$.

Also, there exists $\zeta = \zeta(\epsilon)$ such that

$$P \left(\inf_{\|x\|_E \leq M} \inf_{d(\omega, \hat{g}_{\oplus}(x, t_0)) > \epsilon} \hat{G}_{\oplus}(\omega, x, t_0) - \hat{G}_{\oplus}(\hat{g}_{\oplus}(x, t_0), x, t_0) \geq \zeta \right) = 1.$$

(U3) With $\mathcal{B}_{\delta}(m_{\oplus}(x, t))$ and $N(\epsilon, \mathcal{B}_{\delta}(m_{\oplus}(x, t)), d)$, as defined in Assumption 7

$$\int_0^1 \sup_{\|x\|_E \leq M} \sqrt{1 + \log N(\epsilon, \mathcal{B}_{\delta}(m_{\oplus}(x, t)), d)} d\epsilon = O(1) \text{ as } \delta \rightarrow 0.$$

(U4) There exist constants $\tau > 0, D > 0$ such that, for any given t_0 ,

$$\inf_{\|x\|_E \leq M} \inf_{d(\omega, m_{\oplus}(x, t_0)) < \tau} M_{\oplus}(\omega, x, t_0) - M_{\oplus}(m_{\oplus}(x, t_0), x, t_0) - D d(\omega, m_{\oplus}(x, t_0)) \geq 0.$$

A4 Proofs for Section 4

We use $\mu_{0j} = E(K_h(T - t_0)(T - t_0)^j)$ and $\tau_{0j} := E(K_h(T - t_0)(T - t_0)^j | Y = y)$.

Lemma 5.

$$\begin{aligned}\mu_{0j} &= h^j \left[f_{X,T}(x, t_0) K_{0j} + h K_{0(j+1)} \left(\frac{\partial}{\partial t} f_{X,T}(x, t) \right) \Big|_{t=t_0} + O(h^2) \right], \\ \tau_{0j} &= h^j \left[f_{X,T|Y}(x, t_0, y) K_{0j} + h K_{0(j+1)} \left(\frac{\partial}{\partial t} f_{X,T|Y}(x, t, y) \right) \Big|_{t=t_0} + O(h^2) \right].\end{aligned}$$

This holds for all x , and in the case of τ_{0j} , the error term is uniform over all $y \in \Omega$.

Proof. This follows from a second-order Taylor expansion in the second argument at $t = t_0$, under the assumption that the densities exist and are twice continuously differentiable in the T -direction for all $X = x$. \square

Proof of Proposition 3. Observe that

(i) Since $\mu = E_{X|T}(X)$ and recalling (4), $E_{X,T}(s_1(X, x, T, t_0, h)) = 0$, we have,

$$\begin{aligned}& \int d^2(y, \omega) s_1(z, x, t, t_0, h) dF_{X,T,Y}(z, t, y) \\ &= \int d^2(y, \omega) \left(\int s_1(z, x, t, t_0, h) dF_{(X,T)|Y}(z, t, y) \right) dF_Y(y) = 0.\end{aligned}$$

(ii) By a similar argument as Lemma 2 and using Lemma 5 we find

$$\begin{aligned}\int s_2(t, t_0, h) dF_{X,T|Y}(x, t, y) &= \int \frac{1}{\sigma_0^2} K_h(t - t_0) (\mu_{02} - (t - t_0)\mu_{01}) dF_{X,T|Y}(x, t, y) \\ &= \frac{\tau_{00}(y) \mu_{02} - \tau_{01}(y) \mu_{01}}{\sigma_0^2} = \frac{f_{X,T|Y}(x, t_0, y)}{f_{X,T}(x, t_0)} + O(h^2) \\ &= \frac{dF_{Y|(X,T)}(y, x, t)}{dF_Y(y)} + O(h^2).\end{aligned}$$

Hence, proceeding similarly as in Proposition 2,

$$\begin{aligned}
& \int d^2(y, w) s^G(z, x, t, t_0, h) dF_{X, T, Y}(x, t, y) \\
&= \int d^2(y, w) s_1(z, x, t, t_0, h) dF_{X, T, Y}(x, t, y) + \int d^2(y, w) s_2(t, t_0, h) dF_{X, T, Y}(x, t, y) \\
&= \int d^2(y, w) \left(\frac{dF_{Y|X, T}(y, x, t)}{dF_Y(y)} + O(h^2) \right) dF_Y(y) \\
&= M_{\oplus}(\omega, x, t_0) + O(h^2).
\end{aligned}$$

Thus, minimizing \tilde{G}_{\oplus} is approximately the same as minimizing the conditional Frechet function M_{\oplus} . Since the error term is uniform over $y \in \Omega$ by assumptions (B3)-(B4) concerning the existence and uniqueness of the minimizer of the respective objective functions, we have $d(m_{\oplus}(x, t_0) - \tilde{g}_{\oplus}(x, t_0)) = o(1)$ as $h = h_n \rightarrow 0$. The rate of convergence, hence the result follows using a similar technique as in the proof of Theorem 3 in Petersen and Müller (2019). \square

Proof of Proposition 4. Using the empirical weight function defined in (19)- (22),

$$\hat{s}_{il} = K_h(T_{il} - t_0)(X_{il} - \bar{X}_l)^T \hat{\Sigma}_{20}^{-1}(x - \bar{X}_l) + \frac{1}{\hat{\sigma}_0^2} [K_h(T_{il} - t_0)\hat{\mu}_{20} - (T_{il} - t_0)\hat{\mu}_{10}].$$

and a set of auxiliary weight parameters

$$s_{il} = K_h(T_{il} - t_0)(X_{il} - \mu)^T \Sigma_{20}^{-1}(x - \mu) + \frac{1}{\sigma_0^2} K_h(T_{il} - t_0) [\mu_{20} - (T_{il} - t_0)\mu_{10}].$$

we observe that ,

$$\hat{s}_{il} - s_{il} = (U_0 K_h(T_{il} - t_0) + U_1^T X_{il} K_h(T_{il} - t_0)) + (V_0 K_h(T_{il} - t_0) + V_1 K_h(T_{il} - t_0)(T_{il} - t_0)),$$

where

$$\begin{aligned} U_0 &= U_0(x) := \bar{X}_l^T \Sigma_{20}^{-1}(x - \bar{X}_l) - \mu^T \Sigma_{20}^{-1}(x - \mu); & V_0 &= V_0(t_0, h) := \frac{\hat{\mu}_{02}}{\hat{\sigma}_0^2} - \frac{\mu_{02}}{\sigma_0^2}; \\ U_1 &= U_1(x, t_0, h) := \Sigma_{20}^{-1}(x - \mu) - \hat{\Sigma}_{20}^{-1}(x - \bar{X}); & V_1 &= V_1(t_0, h) := \frac{\hat{\mu}_{10}}{\hat{\sigma}_0^2} - \frac{\mu_{10}}{\sigma_0^2}. \end{aligned}$$

Then the difference $\hat{G}_\oplus(\omega) - \tilde{G}_\oplus(\omega)$ can be written as

$$\begin{aligned} \hat{G}_\oplus(\omega) - \tilde{G}_\oplus(\omega) &= \frac{1}{n} \sum_{i=1}^n \left(\frac{1}{n_i} \sum_{l=1}^{n_i} [\hat{s}_{il}(x_0, t_0, h) - s_{il}(x_0, t_0, h)] d^2(Y_{il}, \omega) \right) \\ &\quad + \frac{1}{n} \sum_{i=1}^n \left(\frac{1}{n_i} \sum_{l=1}^{n_i} [s_{il}(x_0, t_0, h) d^2(Y_{il}, \omega) - E(s_{il}(x_0, t_0, h) d^2(Y_{il}, \omega))] \right). \end{aligned} \tag{31}$$

Note that $\bar{X}_l = O_P(n^{-1/2})$ implies $U_0 = O_P(n^{-1/2})$ and $\hat{\Sigma}_{20} = O_P((nh)^{-1/2})$. Hence $\|U_1\|_E = O_P((nh)^{-1/2})$. Using Lemma 5 we have, $V_0 = O_P((nh)^{-1/2})$, $V_1 = O_P((nh^3)^{-1/2})$. Since

$$\begin{aligned} E(K_h(T_{il} - t_0)(T_{il} - t_0)^j d^2(Y_{il}, \omega) X_{il}) &= O(h^j), \\ E(K_h^2(T_{il} - t_0)(T_{il} - t_0)^{2j} d^4(Y_{il}, \omega) X_{il}) &= O(h^{2j-1}), \end{aligned}$$

the first term in the above equation is $O_P((nh)^{-1/2})$ and also, $E(s_{il}^2(x, t_0, h)) = O(h^{-1})$ which implies that the second term in equation (31) is also $O_P((nh)^{-1/2})$. Thus we have $\hat{G}_\oplus(\omega) - \tilde{G}_\oplus(\omega) = o_p(1)$ for any $\omega \in \Omega$ as $nh \rightarrow \infty$. Following the same arguments as in the proof of Proposition 2 the claim follows and then Theorem 2, using Propositions 3 and 4. \square

Proof of Theorem 3. For any given local point t_0 in the T -direction, consider the process, $\{Z_n(x) := d(\hat{g}_\oplus(x, t_0), m_\oplus(x, t_0)); x \in \mathbb{R}^p : \|x\|_E \leq M \text{ for some } M > 0\}$. From Theo-

rem 2, $Z_n(x) = o_P(1)$. To show the uniform convergence of $\{Z_n(x)\}$ using Theorem 1.5.4 of [Van Der Vaart and Wellner \(2000\)](#) we need to show the asymptotic equicontinuity of $\{Z_n(x)\}$, that is, for any $S > 0$ and $\delta \rightarrow 0$,

$$\limsup_{n \rightarrow \infty} P \left(\sup_{\substack{\|x-y\|_E < \delta \\ \|x\|_E \leq M, \|y\|_E \leq M}} |Z_n(x) - Z_n(y)| > 2S \right) \rightarrow 0.$$

Since,

$|Z_n(x) - Z_n(y)| \leq d(\hat{g}_\oplus(x, t_0), \hat{g}_\oplus(y, t_0)) + d(m_\oplus(x, t_0), m_\oplus(y, t_0))$, it suffices to show that $m_\oplus(x, t_0)$ is uniformly continuous for $\|x\|_E \leq M$ and for any $S > 0$ and $\delta \rightarrow 0$,

$$\limsup_{n \rightarrow \infty} P \left(\sup_{\substack{\|x-y\|_E < \delta \\ \|x\|_E \leq M, \|y\|_E \leq M}} d(\hat{g}_\oplus(x, t_0), \hat{g}_\oplus(y, t_0)) > 2S \right) \rightarrow 0.$$

We observe that, for $\delta > 0$ and $x, y \in \mathbb{R}^p$ with $\|x - y\|_E < \delta$,

$$\begin{aligned} \sup_{\omega \in \Omega} |M_\oplus(\omega, x, t_0) - M_\oplus(\omega, y, t_0)| &= \sup_{\omega \in \Omega} |\tilde{G}_\oplus(\omega, x, t_0) - \tilde{G}_\oplus(\omega, y, t_0)| \\ &= \sup_{\omega \in \Omega} |E \left((s^G(X, x, T, t_0, h) - s^G(X, y, T, t_0, h)) d^2(Y, w) \right)| \\ &= \sup_{\omega \in \Omega} |E \left(((X - \mu)^T \Sigma_{20}^{-1}(x - y)) d^2(Y, w) \right)| \rightarrow 0 \text{ as } \delta \rightarrow 0. \end{aligned}$$

This, combined with Assumption (U1) implies that, for any given t_0 , $m_\oplus(x, t_0)$ is continuous at every x in the compact set where $\|x\|_E \leq M$, hence is uniformly continuous over $\{x \in \mathbb{R}^p : \|x\|_E \leq M\}$. Finally, to show the asymptotic equicontinuity of $d(\hat{g}_\oplus(x, t_0), \hat{g}_\oplus(y, t_0))$, let us assume, for any $\epsilon > 0$ and $\|x\|_E, \|y\|_E \leq M$, $d(\hat{g}_\oplus(x, t_0), \hat{g}_\oplus(y, t_0)) > \epsilon$. Then using the form of the corresponding objective function, $\hat{G}(\omega, x, t_0)$, we have,

$$\sup_{\substack{\|x-y\|_E < \delta \\ \|x\|_E \leq M, \|y\|_E \leq M}} \sup_{\omega \in \Omega} |\hat{G}(\omega, x, t_0) - \hat{G}(\omega, y, t_0)| = O_P(\delta).$$

However, this is a contradiction to Assumption (U1) as $\delta \rightarrow 0$ and thus first result follows. Also, we observe that $U_0(x)$ and $U_1(x, t_0)$, as described in the proof of Proposition 3, are respectively $O_P(n^{-1/2})$ and $O_P((nh)^{-1/2})$, uniformly over $\|x\|_E \leq M$. Thus the result concerning uniform rate of convergence of $\hat{g}(x, t_0)$ for $\|x\|_E \leq M$, can be proven following a similar line of argument as in Theorem 2 of Petersen and Müller (2019). \square

A5 Additional Data Illustration - Impact of GDP on human mortality

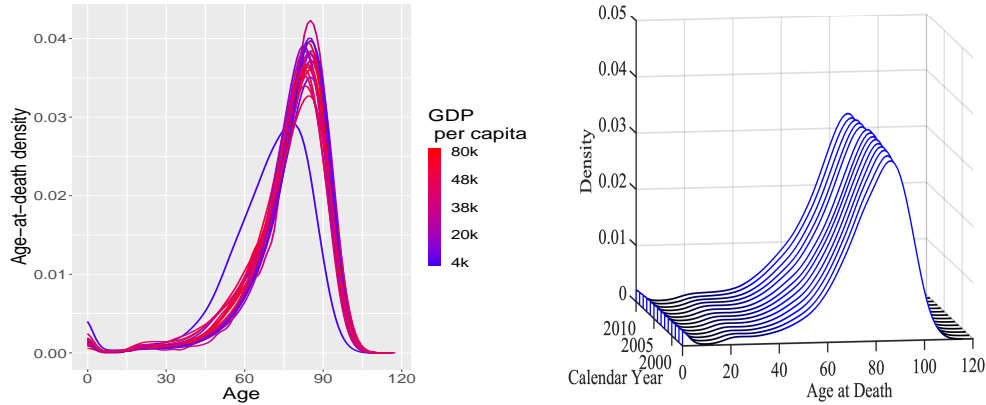


Figure A5: Visualization of the mortality data. The left panel displays the observed age-at-death densities for 22 countries for the calendar year 2005. The color of the densities indicates the transition from lower GDP per capita (blue) to higher GDP per capita (red), where a shift of densities to the right signals enhanced longevity. The right panel is the 3D image plot of the time-varying age-at-death distribution for the US, visualized as time-varying density over 14 calendar years.

We demonstrate the estimation and efficacy of the proposed Concurrent Object Regression (CORE) model in view of another real data application. To this end we consider demographic data, where one often encounters life tables for different countries over many calendar years, viewed here as random realizations of age-at-death distributions that can be visualized as densities. It is important to observe that the space of densities \mathcal{F} is not a vector space. However, densities, as random objects, reside in a metric space, equipped with a suitable metric. Of interest is to see if certain economic indices are associated with age-at-death distributions at the country level. The age-at-death distribution is expected to change over the calendar years as longevity of the population generally improves, due to improving hygiene, health services and nutrition. We aim to study the dependence of the age-at-death distribution of a country on time (calendar years) and some economic index that also varies over time. We apply both the Nonparametric and Partially Global CORE models to ascertain any such relationship.

Data description : The Human Mortality Database (<https://www.mortality.org/>) provides yearly life table data differentiated by gender for 37 countries across 50 years. For our analysis, we considered the life tables for males according to yearly age-groups varying from age 0 to 120 for 22 countries over 14 calendar years, 1997-2010. Life tables can be viewed as histograms, which then can be smoothed with local least squares to obtain smooth estimated probability density functions for age at death. We carried this out for each year and country, using the Hades package available at <https://stat.ucdavis.edu/hades/> for smoothing the histograms with a choice of the bandwidth as 2 to obtain the age-at-death densities. Thus these data can be viewed as a sample of time-varying univariate probability distributions, for a sample of 22 countries, where the time axis represents 14 calendar years and the observations made at each calendar year for each country correspond to the age at death distribution, over the age interval $[0, 120]$, for that year. An illustration of the time-varying age at death distributions represented as density functions over the calendar years for four selected countries is in Figure A5. The data on GDP per capita at current prices is available at the World Bank Database at <https://data.worldbank.org>.

Estimation using the CORE models : Considering the observed age-at-death densities for the countries over the calendar years as time-varying random objects that reside in the space of distributions equipped with the Wasserstein-2 metric, and GDP per capita for these countries as real-valued time-varying covariates, we fit the proposed Concurrent Object Regression (CORE) models as described in Section 3 and 4.

Figure A6 illustrates the time-varying nature of the fitted Nonparametric CORE model, as per (11). We observe that for a fixed calendar year t_0 the fitted densities appear to shift towards the right as the value of the covariate GDP increases, thus indicating that GDP per capita is positively associated with longevity at a fixed calendar year. If

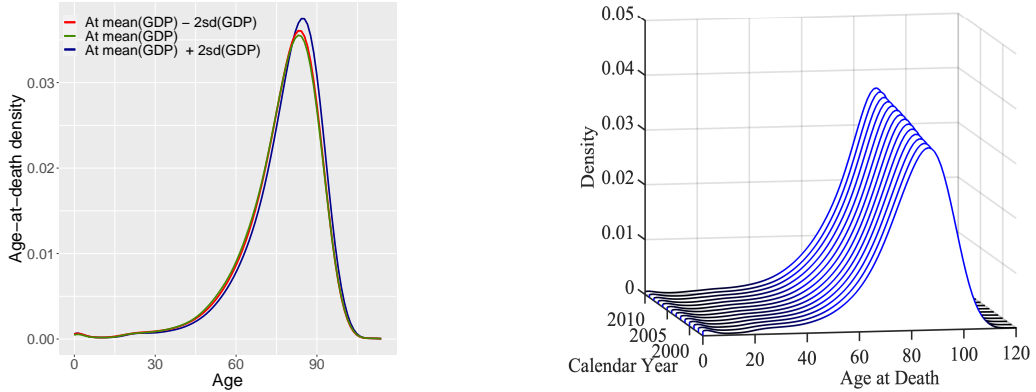


Figure A6: Fitting the Nonparametric Concurrent Object Regression (CORE) model in (11). In the left panel, the locally fitted densities of human mortality distributions, at the year $t_0 = 2005$ and GDP value $x_0 = \text{mean}(\text{GDP}) - 2 \times \text{sd}(\text{GDP})$, $x_0 = \text{mean}(\text{GDP})$ and $x_0 = \text{mean}(\text{GDP}) + 2 \times \text{sd}(\text{GDP})$ are displayed in red, green and blue lines respectively. The right panel shows the fitted densities for the U.S., varying over the years 1997-2010.

alternatively moving along the calendar years for a fixed GDP-value, one again observes an increasing trend in longevity.

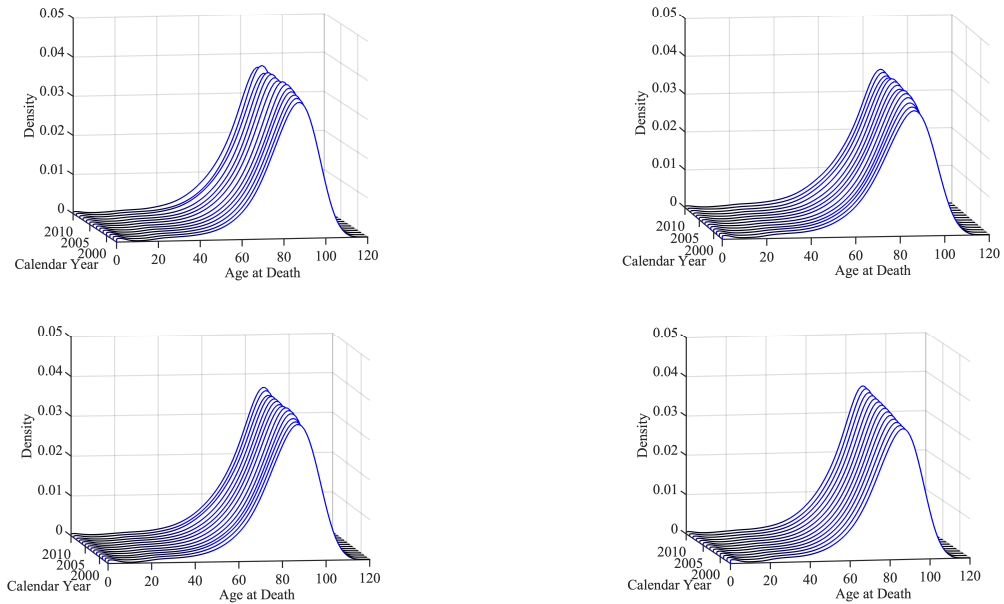


Figure A7: Estimated age at death density functions over the years for males in Australia, Finland, U.S. and Portugal, clockwise in the four panels, starting at the upper left.

Figure A7 shows the 3D plots for the fitted densities over the years for four countries-

Australia, Finland, Portugal and the U.S. We find that over the calendar years the modes for the age-at-death densities are shifted towards older age and that the probability of death before age 5 declines for all the four countries, indicating increasing life expectancy. Also, we notice that, for example, U.S. improves on child mortality over the years while for Finland it remains low throughout. These fits seem to match the observed densities in Figure A8 quite well.

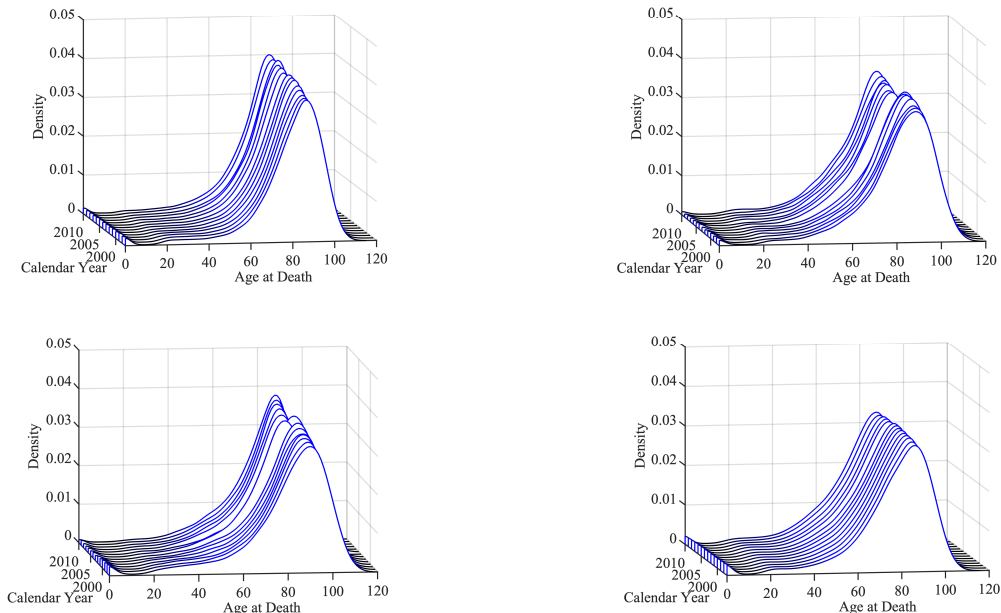


Figure A8: The observed time-varying age at death density functions over the years for males in Australia, Finland, U.S. and Portugal, clockwise in the four panels, starting at the upper left.

We also fitted the Partially Global CORE, as defined in (17), to the same data and compared their performance, where the effect of GDP is modeled as linear and the effect of calendar year as nonparametric. The left panel of Figure A9 indicates that the fits are very similar at randomly chosen points $x_0 = \text{mean}(\text{GDP})$; $t_0 = 2005$.

For both models, the bandwidth h is chosen by leave-one-out cross validation method, as the minimizer of the mean discrepancy between the regression estimates and the ob-

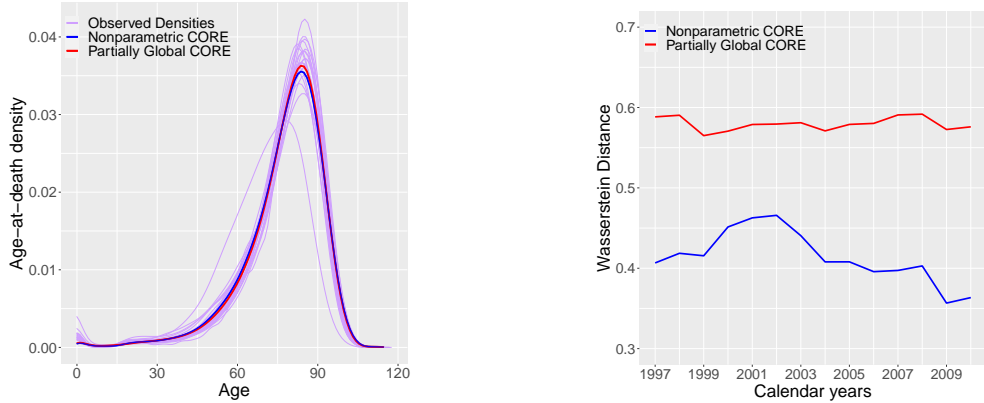


Figure A9: Comparing the fits of Partially Global (17) and Nonparametric (11) Concurrent Object Regression (CORE) models. The left panel shows the local fits at the points $x_0 = \text{median}(X)$, $t_0 = 2005$, comparing both models. The blue and red curves represent the Nonparametric and the Partially Global regression fits, respectively. The purple curves in are the observed densities for the year 2005. In the right panel the average Wasserstein distances between the fitted and the observed densities across the calendar years for the Nonparametric model (blue) and the Partially Global model (red) are illustrated.

served age-at-death density functions and a Gaussian kernel is used. To investigate the comparative goodness-of-fit of the two models further, we computed the average deviation of the fitted from the observed densities for each of the 14 calendar years,

$$\text{MSE}_\oplus(t) := d_W^2(f_\oplus(t), \hat{f}_\oplus(t)), \quad (32)$$

$f_\oplus(t)$ and $\hat{f}_\oplus(t)$ being the observed and fitted age-at-death densities, respectively, at calendar years $t \in \{1997, \dots, 2010\}$ and $d_W(\cdot, \cdot)$ the Wasserstein-2 distance between two densities (distributions). Deviation (32) is displayed in the right panel of Figure 5 for both the Nonparametric and Partially Global CORE models. The Nonparametric model seems to fit the data better, which could indicate that the linear constraint for the impact of GDP imposed in the Partially Global Core model is likely not satisfied. The integrated deviance $\int_{\mathcal{T}} \text{MSE}_\oplus(t) dt$ is 0.413 for the Nonparametric CORE and 0.580 for the Partially CORE, which are not very high, hence validating the fits provided by both models.

A6 Additional Figures for Brain Connectivity in Alzheimer's Disease in Section 6

We present here some additional figures that are referred to in the main paper in Section 6.

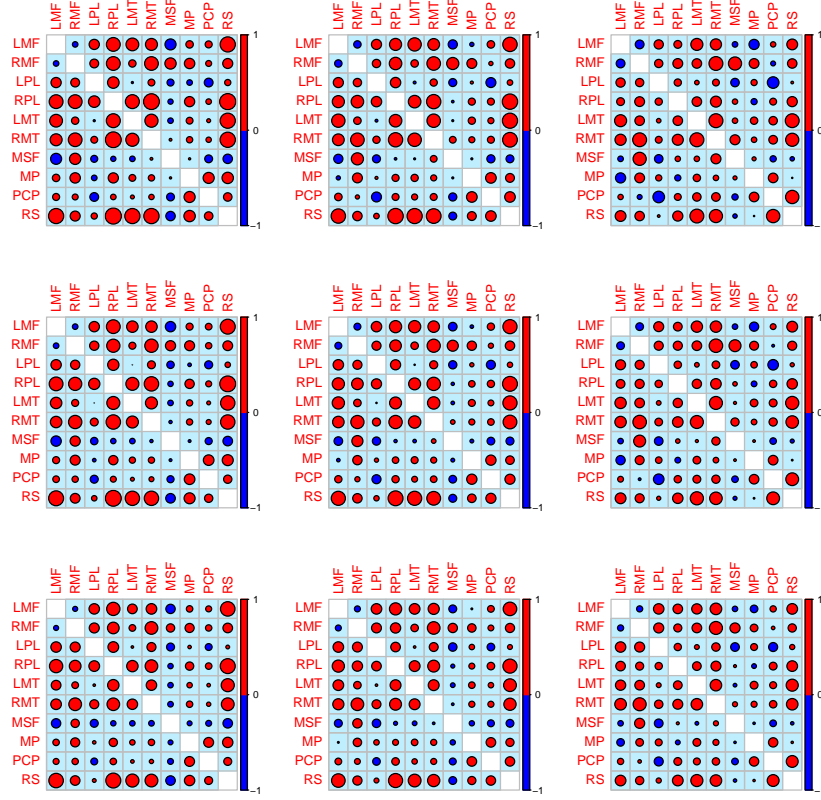


Figure A10: Estimated correlation matrix for the CN subjects fitted locally using Nonparametric CORE in (11) illustrating the dependence of functional connectivity on total cognitive score which gets modulated by age. The arrangement of the panels are the same as that of Figure A2.

Figure A10 displays the connectivity correlation matrices for the CN subjects, estimated using the Nonparametric CORE method locally over a score of different output points. This elicits a the regression relationship between the functional connectivity matrix and the total cognitive scores in Section 6, which is further altered by age. Quite contrary to the case of the AD subjects (A2), here we observe a prominence of positive correlations between the brain parcellation throughout, in terms of stronger magnitude

and higher number. This might well be indicative of a better inter-hub functional connectivity in the CN subjects. Over increasing age we observe a higher value for the total cognitive score which can be associated with a weaker inter-hub connectivity overall. The reduction in Negative Functional Correlation (NFC) for CN subjects is still noted but the evolution is not so drastic over age. In addition, the estimated correlation matrices for the CN subjects exhibit specific patterns of dependency over the connectivity hubs, which, in case of the estimated correlation matrices for the AD subjects is not as discernible. A further application of the Partially Global model gives evidence along the same line as the Nonparametric CORE model (Figure A11). However, the in-sample goodness of fit measured by the integrated deviance statistic (see (27) in Section 6) for the former (0.0056) is marginally better than the latter (0.0071), accounting for a better performance of the Partially Global Model.

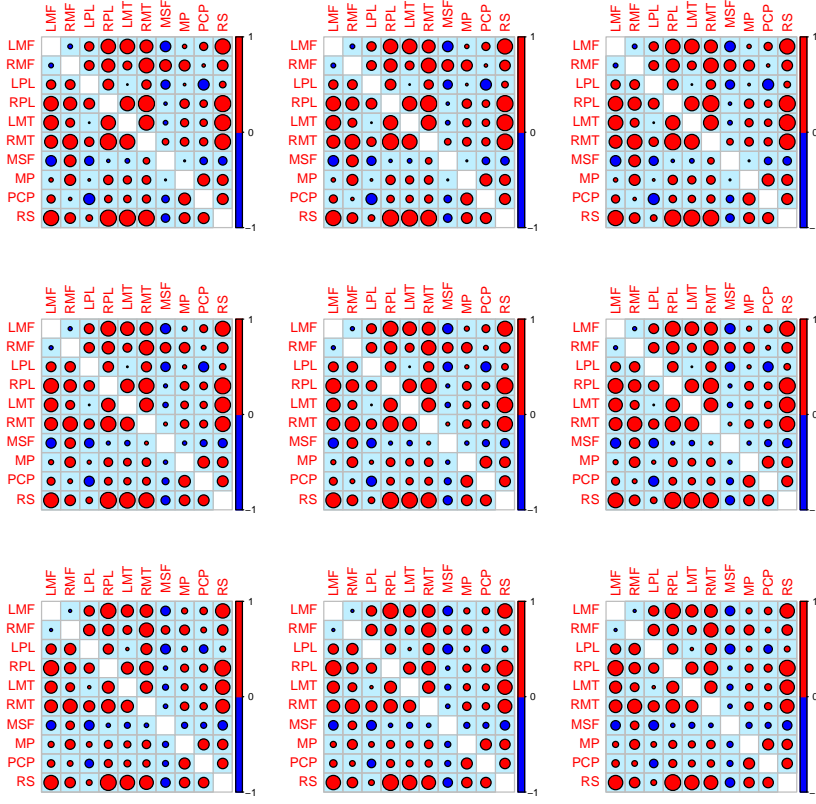


Figure A11: Estimated correlation matrix for the CN subjects fitted locally using Non-parametric CORE in (11) illustrating the dependence of functional connectivity on total cognitive score which gets modulated by age. The arrangement of the panels are the same as that of Figure A2.

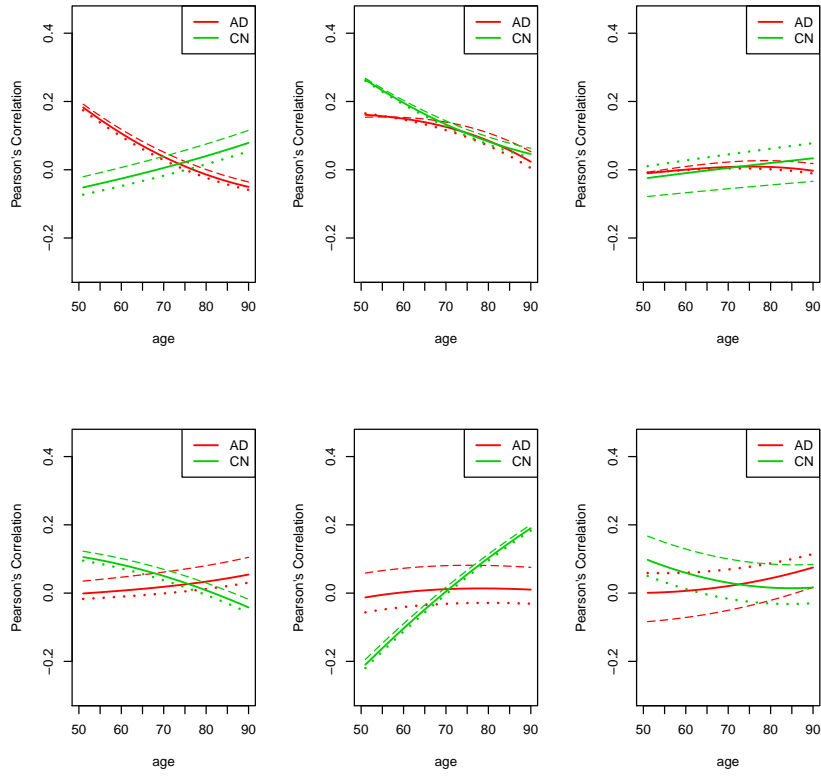


Figure A12: Fitted correlations for varying total cognitive scores and ages across the AD and CN subjects for six chosen connectivity hubs LMF-vs-LPL, RMF-vs-LPL, LPL-vs-RS, PCP-vs-RS, RMT-vs-PCP, MSF-vs-PCP (clockwise in the six panels, starting at upper left). The dashed, solid and dotted lines represent the estimated correlation at $x_0 = 10\%$, 50% , and 90% quantiles of the total cognitive score, respectively, for varying ages. For the CN subjects, the inter-hub correlations appear higher for a lower value of the total cognitive score however, for the AD subjects such pattern is not evident. The correlations get generally weaker with higher age.